AN ABSTRACT OF THE THESIS OF

Gabhriel John for the degree of Master of Science in Forest Ecosystems and Society presented on December 4, 2025.

Title: Douglas-fir and Western Hemlock Responses to Extreme Heat.

Abstract approved:

_____

Christopher J. Still
Mark D. Schulze

The present project uses the 2021 Pacific Northwest Heat Dome as a case study for evaluating the relationships between microclimate metrics and the growth & water use of trees at the HJ Andrews Experimental Forest. We do so while exploring the applications and limitations of statistical tools to process and analyze high-frequency dendrometry data. 2021 was undoubtedly the hottest year recorded at the HJA, and as record-breaking weather events like the Heat Dome are likely to increase in the future, it is increasingly important to understand how they affect the ability of plants and ecosystems to function.

Focusing on instrumented young and old Douglas-firs as well as old western hemlocks, we find evidence of both resilience and vulnerability. When comparing microclimate metrics across a 7-year record of high-frequency data, high temperature and VPD spikes from the Heat Dome coincided with immediate stem contraction for all 11 sampled trees within the same time period. Modeled assessments of Douglas-firs within our sample reveal that this led to a statistically significant decline in basal area increment for most trees lasting at least two weeks after the event in a way that was uncharacteristic of typical mid-summer decreases in growth rate. The extent of growth recovery after 2021 is more variable; basal area increment in subsequent years (2022-2025) has mostly remained low despite a return to more typical climatic conditions, suggesting possible carry-over effects that are also related to ongoing drought. These observations are consistent between assessments based on

dendrometry or dendrochronology, but are statistically insignificant. We suggest that future research continues to build upon this growing body of work at the intersection of climate, canopy ecology, and phenology subcomponents. Further incorporating fine-scale data is sure to increase global understanding of biotic interactions and the disturbance and climate regimes that shape them.

Douglas-fir and Western Hemlock Responses to Extreme Heat

by
Gabhriel John

A THESIS

submitted to

Oregon State University

in partial fulfillment of
the requirements for the
degree of

Master of Science

Presented December 4, 2025
Commencement June 2026

Master of Science thesis of Gabhriel John presented on December 4, 2025

APPROVED:

Co-major Professor, representing Forest Ecosystems and Society

Co-major Professor, representing Forest Ecosystems and Society

Head of the Department of Forest Ecosystems and Society

Dean of Graduate Education

I understand that my thesis will become part of the permanent collection of Oregon State University libraries. My signature below authorizes release of my thesis to any reader upon request.

Gabhriel John, Author

ACKNOWLEDGEMENTS

Data and facilities were provided by the H.J. Andrews Experimental Forest and Long Term Ecological Research (LTER) program, administered cooperatively by Oregon State University, the USDA Forest Service Pacific Northwest Research Station, and the Willamette National Forest. This material is based upon work supported by the National Science Foundation under the grant LTER8 DEB-2025755.

CONTRIBUTION OF AUTHORS

Data analysis and visualization: Gabhriel John, Christopher Still, Mark Schulze

Field work: Gabhriel John, Mark Schulze, Amanda Brackett, Christopher Still

Lab work: Gabhriel John, Amanda Brackett

Manuscript editing: Gabhriel John, Christopher Still, Mark Schulze, Loren Albert, Dustin Gannon, Matthew Powers

Manuscript writing: Gabhriel John

Remote data collection and collation: Gabhriel John, Christopher Still, Mark Schulze

Statistical analysis: Gabhriel John, Dustin Gannon, Christopher Still, Mark Schulze

Study design: Christopher Still, Mark Schulze, Gabhriel John

Study support, advising, and mentorship: Christopher Still, Mark Schulze, Dustin Gannon, Amanda Brackett, Loren Albert, Matthew Powers

TABLE OF CONTENTS

TABLE OF CONTENTS (Continued)

LIST OF FIGURES

LIST OF TABLES

Chapter 1: Manuscript

1.0 Introduction

1.1 Broader problem: climate-related tree stress

Globally, forests are sequestering less carbon from the atmosphere due to stressors imposed by anthropogenic climate change (Davis et al., 2023). This hinders their ability to provide countless ecosystem services including but not limited to wood products, oxygen, wildlife habitat, recreation, and of course carbon sequestration (Batavia & Nelson, 2019; Kunert et al., 2022; Rastogi et al., 2018; Still et al., 2023). Heat waves—acute periods of extremely high temperatures—are just one example of weather events that are increasing with climate change. Heat waves and other anomalous climate events like droughts are projected to increase in frequency, duration, and severity over time (Dai et al., 2013; Duarte et al., 2016; Salomón et al., 2022).

The effects of drought and heat stress have been globally identified and could reshape ecosystems and their functioning (Allen et al., 2010; Hammond et al., 2022). For trees, these effects can result in physical damage, increased vulnerability to pests and pathogens, reduced carbon uptake, reduced fecundity, hydraulic failure in leaves, water loss, and mortality (Allen et al., 2010; Breshears et al., 2021; Kunert et al., 2022; Rastogi et al., 2018; Still et al., 2023b). Forest research is complicated by concurrent intertwined factors involving the tree itself and its environment. For example, it can be challenging to disentangle the effects of heat and drought on tree growth and physiology since these events often occur together. Tree growth and physiology further varies with each tree's specific growing environment such as site, species, and age (Allen et al., 2010; Italiano et al., 2023; Wang et al., 2023).

Although it is difficult to attribute tree growth to specific microclimate variables, some factors are consistently more influential than others; such is the case for vapor pressure deficit (**VPD**), defined as the difference between the current water vapor content in the air and the saturation vapor capacity of that air. Stomatal control of leaf-level gas diffusion is generally negatively correlated with VPD (Grossiord et al., 2020). As a result, high VPD is associated with reduced photosynthesis and net carbon uptake (Jarecke et al., 2023). At its most severe, photosynthesis reductions due

to high VPD can lead to carbon starvation and can possibly lead to hydraulic failure. Temperature strongly affects VPD, as warmer air has a greater capacity to hold water vapor This increases the saturation vapor pressure and potential for a pressure gradient, thereby increasing evaporative demand regardless of actual moisture content in the soil (Restaino et al., 2016). This can lead to increased water loss via transpiration even with stomatal closure (Allen et al., 2010). Moreover, temperature-driven moisture stress can persist even after a rainfall event (Restaino, Peterson, & Littell 2016). In fact, VPD is often the dominant regional driver of drought stress and mortality among forests (Williams et al., 2013). Even though VPD often coincides with periods of low soil moisture, VPD-induced embolism in young and mature trees can occur despite having abundant soil moisture (Novick et al., 2024). For these reasons, joint investigations of VPD, air temperature, and soil moisture can help uncouple heat and drought-related effects on tree growth (Breshears et al., 2013; Breshears et al., 2021; Grossiord et al., 2020). Importantly, high leaf temperature on its own, independent of its impacts on VPD, can also damage plant tissues and affect tree health and function (Still et al., 2023b).

1.2 Relevance in the Pacific Northwest

The American Pacific Northwest (**PNW**) is particularly vulnerable to climate change. Even models that assume low carbon emissions predict that the PNW will experience increased temperatures, heat waves, wildfires, and droughts (Chang et al., 2023). These changes are already being observed, and perhaps the most notable example is the Heat Dome of June 2021, when air temperatures exceeded almost all previous records and anomalies (Heeter et al., 2023; Thompson et al., 2022; Fleishman et al., 2025). This event occurred near the peak of the growing season in western Oregon, thereby influencing patterns of tree productivity, mortality, and regeneration (e.g., Doolittle, 2025; Still et al., 2023b).

Climate change has increased the probability of similarly extreme weather occurring in the future, and heat waves make other forest disturbances more dangerous (Fleishman et al., 2025). These compounding disturbances have the potential to profoundly alter species interactions and ecosystem function such as

biotic modulation of microclimate. For example, increasingly severe summer climate will further reduce the potential for carbon sequestration in the PNW despite the region's high concentration of forests. Two dominant forest species native to the PNW are Douglas-fir (*Pseudotsuga menziezii*) (**DF**) and western hemlock (*Tsuga heterophylla*) (**WH**). DF is shade-intolerant, often establishing after major disturbances and reaching canopy dominant and emergent positions in mature and old growth forest stands (Uchytil, 1991). WH is among the most shade tolerant species, often occupying all vertical strata in old growth stands but also capable of co-occupying the overstory with DF in younger stands (Johnson & Swanson, 2009). Both species retain their leaves year-round, meaning that prolonged hydraulic deficits could lead to further foliar stress and/or damage (Salomón et al., 2022). Further, both DF and WH are heat-sensitive (Kunert et al., 2022), with WH experiencing disproportionately high rates of heat damage (Sibley et al., 2025). This exemplifies the importance of studying how species persist during increasingly hot summers.

1.3 Research Need

As climate patterns across the temperate forest biome change in unprecedented and potentially endangering ways, researchers and forest managers need to understand and predict tree responses to such changes to more accurately and confidently plan carbon budgets, adjust management plans, and assess ecological risk. Despite the increasing likelihood of anomalous climate events like the Heat Dome, it is unlikely that forests can be managed in the short term to mitigate the effects of heat waves (Breshears et al., 2021). More research, then, is imperative and timely as heat-related climate stress threatens the capacity for forests in places like the PNW to provide microclimate refugia and store carbon (Davis et al., 2023; Duarte et al., 2016).

In the four years since the Heat Dome, dozens of papers have focused on its broad-scale effects, particularly in terms of healthcare, climate, and foliar scorch (e.g., Fleishman et al., 2025). The present study presents a novel, high-resolution glimpse into tree expansion before, during, and after the Heat Dome. Such fine-scale data will help unravel the contributing effects of drought and heat, both of which were present

during the Heat Dome. In this case, heat tolerance and the mechanisms that dictate it within both young and old trees are poorly understood because they are easily overshadowed by the droughts that often accompany heat waves (Still et al., 2023b; Yi et al., 2022). Some evidence points to drought-induced stress as the primary culprit of tree stress and mortality during the Heat Dome (e.g., Klein et al., 2022), but high air temperatures were more likely the driver of extensive foliar damage compared to drought conditions (Still et al., 2023b). Moreover, temperature-driven moisture stress can persist even after a rainfall event (Restaino et al., 2016).

One method to understand Heat Dome effects on trees that has not yet been thoroughly utilized in literature is high-resolution dendrometry. When trees sequester carbon, up to 75% of the assimilated biomass is in the stem (Reich et al., 2014). Band dendrometers are devices placed around tree stems that measure incremental girth changes at highly resolved time scales with microscopic precision. Such changes arise due to oscillating cycles of transpiration (resulting in stem shrinkage) and rehydration and/or permanent incremental growth (result in stem expansion or swelling) (Deslauriers et al., 2011; Downes et al., 1999). When paired with site-specific temperature and moisture information, one can use dendrometer data to estimate when water stress and biomass accumulation occur in the tree (Balducci et al., 2019; Downes et al., 1999). Recent (i.e., within the last five years) advancements in statistical software have enabled researchers to more efficiently process and analyze dendrometry data (Haeni et al., 2020; Knüsel et al., 2021; Zweifel et al., 2016). Such advancements have introduced a new area of methodological refinement in the process of analyzing tree growth during specific time periods and/or key events. Our hope is that this work will shed more light on the relative impacts of rainfall versus temperature and VPD regarding the timing and magnitude of tree expansion, an area of inquiry which is currently uncertain (Jarecke et al., 2023).

What is further missing in current Heat Dome literature is the use of high-resolution dendrometry data and its pairing with dendrochronological data. Harrington et al. (2023) measured stem diameter at the end of the 2021 and 2022 growing seasons, finding that diameter prematurely stopped expanding in 2021. In a separate study by Heeter et al. (2023), tree core analysis was used to explain just how

uniquely extreme the 2021 summer heat was. According to a review by Fleishman et al. (2025), other studies have measured primary productivity via vegetation greenness; foliar scorch; and microclimate metrics. These studies found that productivity as measured by greenness was low in 2021 but not anomalously so across the PNW, vegetative scorch was extensive, and VPD & air temperature likely constrained the 2021 growing season more than soil moisture did.

High-resolution dendrometry provides information of within-ring growth timing and its environmental controls, while tree core analysis allows researchers to affirm results from high-resolution dendrometry while contextualizing them into a broader chronology of individual tree growth and the previous climate events that affected growth. There is a large literature on using dendrochronological metrics such as total ring-width, earlywood width, latewood width, and wood density as useful proxies for tree responses to hydroclimatic phenomena (Acosta-Hernández et al., 2020). And because latewood is added during the summer months it is therefore more sensitive than earlywood to periods of stressful temperature, VPD, and soil moisture depletion (Jarecke et al., 2024), and comparison of latewood data to dendrometer data might be particularly revealing.

1.4 Research questions

Based on the aforementioned research gaps, we ask three central questions:
1) How did the 2021 Heat Dome affect western hemlock and Douglas-fir growth at the HJA for the remainder of the 2021 growing season and subsequent years? **2)** Are there specific microclimate variables that correlate with Heat Dome-related growth patterns? **3)** How do the results of 1) and 2) compare to long-term growth trends and climate relationships derived from tree cores?

2.0 Materials and Methods

2.1 Location

This project was centered around the HJ Andrews Experimental Forest (**HJA**) Discovery Trail in Blue River, Oregon (approximate coordinates: 44.1734° N, 122.1968° W). Sites used in this study are mesic temperate conifer forests in a moist

valley with alluvial volcanic soils. The Discovery Trail is dominated by WH and DF of varying age classes. The oldest primary DF trees are between 450-500 years old and 60-70 meters tall. Conversely, younger, secondary forest plantations are younger than 75 years (Swanson, 2023).

2.2 Dendrometer and microclimate data origins

All microclimate and dendrometry data come from two meteorological stations situated 0.72 kilometers apart along the southwestern boundary of the HJA (**Figure 1**).

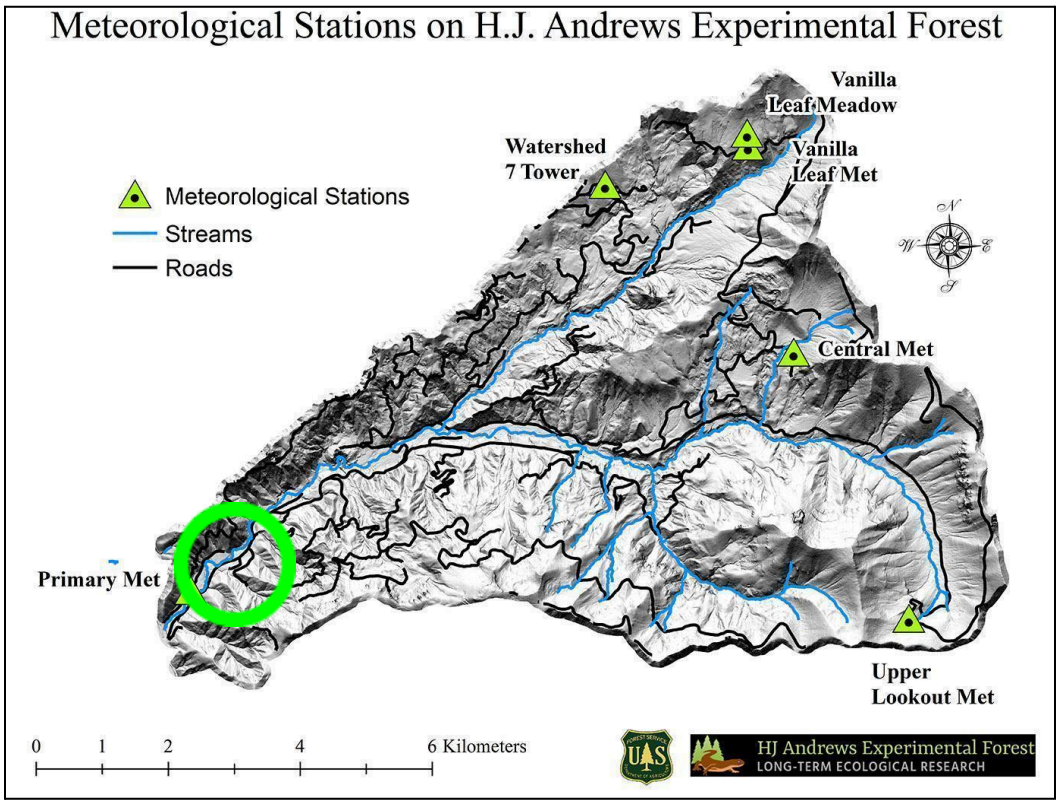

Figure 1: Map of the HJA (Andrews Forest Program via CC-BY, n.d.). Green circle indicates the approximate location of the Discovery Tree Meteorological Station (DSCMET).

The first meteorological station, the Primary Meteorological Station (**PRIMET**), with an elevation of 436 meters, has coordinates of 44.21 N, -122.26 W (dataset MS001, Daly et al., 2025). The site is a maintained clearing at HJA Headquarters surrounded by forest in the bottom of a narrow valley near the mouth of the 6,232-hectare Lookout Creek watershed. PRIMET metrics used for this study include daily air temperature at 1.5m spanning from 1972 to 2025 as well as daily precipitation

spanning from 2019 to 2025. Air temperature comes from two PRIMET datasets; one, hereafter referred to as "PRIMET daily air temperature 'A'" is already presented at a daily resolution and spans from May 1972 to March 2019. The second dataset calculates mean daily air temperature based on high-frequency data from the HJA Provisional Data Portal. Precipitation was measured using a NOAH IV Gage (ETI Instrument Systems, 2020). These measurements (converted from in to cm and from calendar year to water year) were downloaded from the National Atmospheric Deposition Program Precipitation Network, which refers to PRIMET as OR10 (National Atmospheric Deposition Program, 2022). To enable analysis of recent data that had not been published in a final format on the Forest Science Databank or the Environmental Data Initiative archive, all data for this project were downloaded from the Provisional Data Portal with the exception of precipitation and PRIMET daily air temperature "A" (Andrews Forest Program, n.d.). All metrics from the Provisional Portal maintain their original temporal resolution of 5-minute increments unless otherwise noted. NADP data maintain their original daily temporal resolution.

Upper-canopy microclimate measurements were desirable to more accurately reflect conditions experienced by photosynthesizing leaves. Generally, microclimate differs substantially in the upper canopy versus elsewhere in the forest. The upper canopy contains most leaf surface area, and this region is where most of the forest's carbon and water fluxes occur (Still, 2023b). Thus, we also used data from a second meteorological station, the Discovery Tree Meteorological Station (**DSCMET**), with an elevation of 466 meters and coordinates of 44.22 N, -122.25 W (dataset MV005, (Still et al., 2023a)). All DSCMET measurements are recorded as five-minute means on Campbell Scientific CR1000 dataloggers, are streamed hourly to a server via radio telemetry, are subjected to automated QA flagging through a site-specific implementation of the GCE Data Toolbox in MATLAB (Sheldon 2022)and then uploaded onto a provisional data portal. Metrics used for this project include upper canopy fan-aspirated air temperature (℃) measured 56 meters aboveground, VPD (converted from mbar to kPa) measured at the same height, soil water content fraction measured 50 cm belowground, and dendrometer expansion or shrinkage readings (μm).

Dendrometer readings come from 11 Ecomatik DC3 automated band dendrometers installed on trees within 25 meters of the base of the Discovery Tree. These dendrometers measure stem circumference changes in micrometers (Entwurf, 2019). The Ecomatik dendrometer sample includes three OG DF (tree IDs 309, 310, 311), four second-growth (**2G**) DF (tree IDs 654, 655, 656, 860), three OG WH (tree IDs 646, 648, 652), and one OG western red cedar (*Thuja plicata*) (tree ID 651). Each dendrometer wraps around a tree stem at approximately breast height (1.5-2 meters above the ground) except for the dendrometer installed on tree ID 309, which surrounds the bole mid-canopy at 43 meters above the ground. Data from the HJA have high temporal resolution, which allows us to understand tree performance before, during, and after the Heat Dome. Dendrometers meas

readings are recorded onto a Campbell Scientific CR1000 datalogger, which rounds the readings to the nearest whole number and has an accuracy of ±0.12%. All dendrometers were installed in mid-July 2018 except for IDs 648, 651, and 652, which were installed in early April 2023. Because of the lack of data for most of the 2018 GS, no data from 2018 were analyzed. The dendrometer for ID 860 was installed in late May 2019, so 2019 data for ID 860 were omitted in analyses that required a full growing season.

2.3 Dendrometer data consolidation, cleaning, and unit conversion

Data on the Provisional Data Portal are separated by year and data set. They have been subjected to automated quality assessment and control routines through the GCE toolbox in Matlab, producing flagged values that must be evaluated by the data user before analysis (ESIP EnviroSensing Cluster, 2014; Sheldon et al., 2013). These routines are well-developed for climate data but not for dendrometer data. For each dendrometer, raw data from all available years in the Provisional Portal were combined in R version 4.4.2, then readings were plotted (R Core Team, 2024; Wickham et al., 2019; Müller, 2020) (**Figure 2**). This was done to visually identify artifacts in the record that did not reflect true bole expansion or contraction and would therefore require manual adjustment. Artifacts may arise from physical bumps to the dendrometer (i.e., from a tree climber, animal, falling branch, or snowfall) or resets

(i.e., a dendrometer potentiometer, with a limited capacity, must be manually reset prior to reaching that limit to maintain continuous measurements). In our time record, loss of power led to data gaps in some years. For tree ID 311 in 2019, failure to reset the band in time led to a gap in recordings during the active GS.

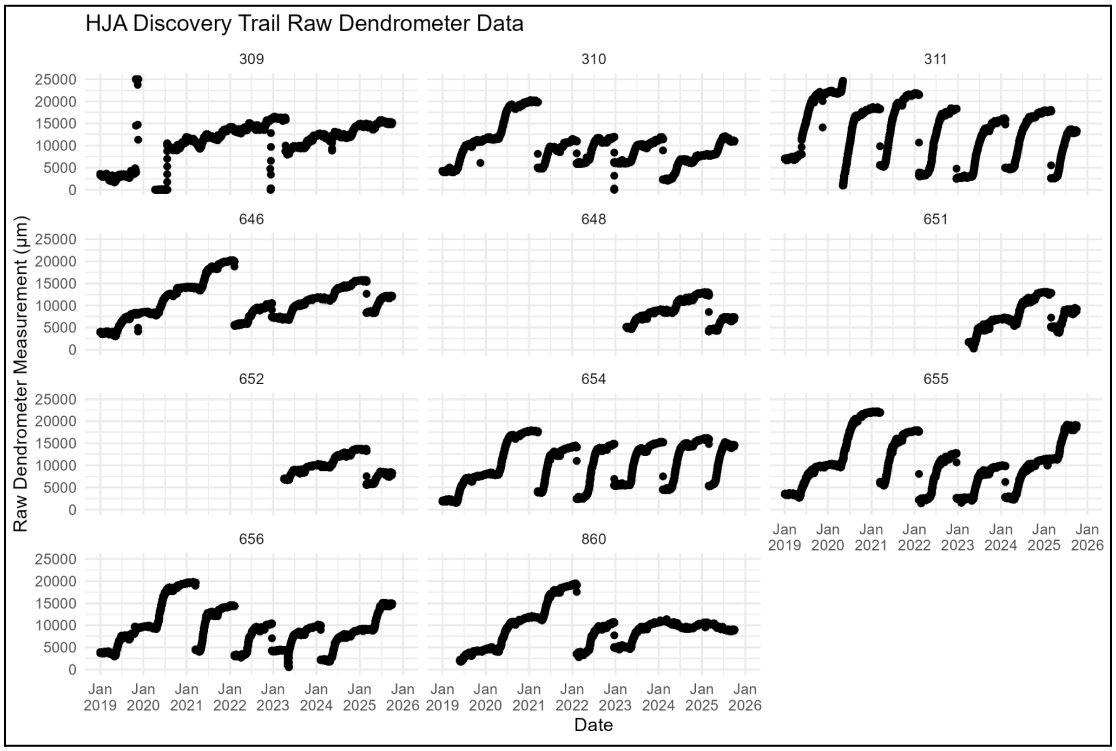

Figure 2: Plots of raw dendrometer data for all 11 dendrometers used in this study. Instrumented trees include three Old-Growth Douglas-firs (tree IDs 309, 310, 311), four second-growth Douglas-firs (tree IDs 654, 655, 656, 860), three old-growth western hemlocks (tree IDs 646, 648, 652), and one old-growth western red cedar (tree ID 651). Green circles represent examples of artifacts that were manually removed before analysis.

Raw data were plotted to visually identify instances of band resets and potential artifacts (**Figure 2**). In Microsoft Excel, each potential artifact was identified if the raw measurements deviated by more than ±1 mm within a 5-minute period. If bumps were consistent across multiple sampled trees, it is likely that the bump reflects unusual yet real expansion. This can happen as tree trunks swell in response to heavy rainfall, especially those occurring after prolonged summer dry spells or during the initial wet-up in the fall months. If a bump was unique to one tree and seemed to be a true artifact, it was manually removed from the record and replaced with an NA value. Further, a new column was added to annotate each period between resets. An example of this framework is included in **Table 1**.

The data were then uploaded back into R and converted to circumference (mm) using an R script that automates the conversion formula outlined in the Ecomatik manufacturer's user manual and accompanying Excel conversion program (Entwurf, 2019). This calculated circumference was finally converted to basal area increment (**BAI**, cm^2). The R script skips missing rows, and each dendrometer required a separate conversion for each period defined by the manual flag annotations. The conversion formula requires the initial circumference (mm) and the first valid dendrometer reading (mm). As such, each period conversion required the last circumference measurement from the period before as well as the first valid dendrometer reading of the new period.

Timestamp (Y-M-D H:M:S)	Raw Value (µm)	Manual flag	Notes
2019-01-01 00:00:00	9165	A	
2019-01-01 00:05:00	9160	A	Last stable reading prior to manual reset
2019-01-01 00:10:00	NA	A	Removed (5489)
2019-01-01 00:15:00	2165	B	First stable reading after reset
2019-01-01 00:15:00	2163	B	

Table 1: Example workflow of conducting quality control checks on raw dendrometer data

After circumference conversions, a new column was added to represent the difference between the circumference value at one time stamp and the circumference value at the time stamp immediately after it. If a difference greater than ±1 mm in a 5-minute period was observed, the raw data at that time stamp was rechecked using the same artifact protocol as above.

2.4 Dendrometer data processing, analysis, and visualization

Cleaned and converted dendrometer data were primarily analyzed and visualized using the R package "dendRoAnalyst" version 0.1.5 (Aryal et al., 2020). DendRoAnalyst has a function to clean data with artifacts included, but we opted for manual cleaning to preserve accuracy and avoid the potential removal of rain response bumps. Daily statistics, including daily maximum and minimum circumference, daily circumference amplitude, and the corresponding times for these

values, were calculated with the daily.data() function in denRoAnalyst. This first required averaging dendrometer data to a daily resolution, which was done with the dendro.resample function.

2.5 Microclimate data cleaning, processing, analysis, and visualization

Microclimate data were uploaded into R, and a script was run to identify the presence and time stamps of quality control flags within our timeframe of interest (January 2019 through September 2025) unless stated otherwise. **Table 2** below summarizes and defines how flags appeared in the datasets for each metric and how we handled them. Precipitation data is not included as flags were not provided. After visually inspecting the distribution of flags, no data were removed based on flags alone; most "Q" flags, for example, showed up during the Heat Dome. This suggests that the conditions during that time were so extreme that their records were flagged as questionable even though they were real. There were also many "Q" and "F" flags for daily air temperature congregated within entire years in the PRIMET dataset starting in 1972.

HJA Microclimate Metric (number of observations)	**QA/QC Flags (number of times present)**	**Percent of total data flagged**	**Percent of total data flagged (excluding M, MII)**
Mean DSCMET air temp at 56m (701,589)	M (28,176) MII (11,883) Q (37) V (1)	5.72%	0.0054%
Mean DSCMET VPD at 56m (701,589)	M (41,988) Q (531) V (1)	6.06%	0.076%
DSCMET SWC at 50 cm (709,921)	M (25,829)	3.64%	0%
Max PRIMET daily air temp at 1.5m (May 1972 - Dec. 2018) (27,228)	E (113) F (346) M (710) Q (600)	6.50%	3.89%
Max PRIMET daily air temp at 1.5m (710,779)	E (19) M (10,367) Q (70) V (1)	1.47%	0.013%

Table 2: QA/QC flags associated with relevant microclimate metrics. E flags refer to estimated values; F flags refer to daily values based on the maximum 15-minute mean value; M and MII flags refer to missing values; Q flags refer to questionable values; V flags indicate a value change from the value before.

Some metrics used in our analyses were calculated from the microclimate data. For example, critical VPD (Breshears et al., 2013) and temperature (Breshears et al., 2021) thresholds for lethal or sublethal plant stress are discussed in the literature, and stress hours (i.e., cumulative hours above a threshold) quantify and visualize conditions that exceed such thresholds. We calculated stress degree hours (**SDH**) (Brackett et al., 2024) by taking hourly averages of mean upper-canopy air temperature, removing missing values, and subtracting our high temperature stress threshold value from each hourly average temperature. All negative values were replaced with 0. Our SDH threshold was 35 ºC based on literature reports of sunlit leaf temperature being typically elevated 3-7K above air temperature (Still et al., 2019) and photosynthesis declining at or closely beyond this temperature for many plant species (Kunert et al., 2022).

We applied a similar SDH methodology to introduce the concept of stress VPD hours (**SVH**). For SVH and all other uses of VPD, we converted VPD from mb to kPa. Our stress VPD threshold was defined as 3 kPa based on modeled and observed declines in photosynthesis at or closely beyond this point (Marks et al., 2024). We also utilized the hydrometeorological dryness index (**HDI**) (Martin et al., 2017), which represents the ratio of atmospheric VPD divided by the volumetric water content of soil at 50 cm. HDI, with units of kPa $m^{-3}H_2O$ m^3soil, represents a site's atmospheric moisture demand and its concurrent soil moisture availability to try and capture the combined moisture stress of a tree at a given time. HDI is a usefulalternative to other metrics that capture atmospheric and soil water stress but require more than two measurements. We introduce stress HDI hours (**SHH**) and define its stress threshold in a different way from SDH and SVH. We divided our SVH threshold (3 kPa) by the 10th percentile of soil water content (**SWC**) fraction, a common threshold used when studying drought effects on vegetation suppression (Li et al., 2023). We specifically used the 10th percentile of SWC at 50 cm since that

depth is used for HDI calculations. The quotient of this division rounds up to 35 kPa $m^{-3}H_2O$ m^3soil.

Most data visualizations are based on annual accumulations. This was done by adding a "year" factor column to each relevant dataset, grouping by year, and subtracting the first value for each year from the column of interest. The result is that the data for each year start at 0 on the same figure to more easily see how microclimate variables and tree growth vary from year to year. The color palette "turbo" from the R package "viridis" was chosen for annual plots to maximize accessibility (Garnier et al., 2024). The R package "ggrepel" version 0.9.6 was also used to make visibility clearer (Slowikowski, 2024).

2.6 Tree core collection and processing

After the 2024 GS, tree cores were collected from WH and DF trees to assess water use and stress among trees over a longer period, especially during prior heat waves and drought events. Sample trees were chosen because they either had an Ecomatik dendrometer or a manual band dendrometer installed on the lower bole. Based on similar methodologies (e.g., Acosta-Hernández et al., 2020), we collected 2 ~5 mm cores at breast height from each sample tree. **Table 3** below includes the ID, site, species, and average dbh of each sample tree. All trees are on the same alluvial terrace at the bottom of Lookout Creek drainage.

Tree ID	Site ID	Species	DBH (cm)
654	**DT**	**WH**	**29.5**
646	**DT**	**WH**	**64.4**
648	**DT**	**WH**	**66.9**
647	DT	WH	27
2566	DT	WH	68
4662	DT	WH	58.7
3495	DT	WH	59
652	**DT**	**WH**	**48.5**
309	**DT**	**DF**	**126.5**
310	**DT**	**DF**	**120**
311	**DT**	**DF**	**102**
860	**DT**	**DF**	**29**

655	**DT**	**DF**	**34.1**
656	**DT**	**DF**	**41.9**
657	DT	DF	40.2
5461	HQSWP	DF	58.4
2838	HQSWP	DF	43.05
2577	HQSWP	DF	45.8
4744	HQSWP	DF	42.5
655	HQSWP	DF	37.1
638	HQRIP	DF	44
640	HQRIP	DF	50.1
3354	HQRIP	DF	43.8
461	HQRIP	DF	47

Table 3: Tree core metadata recorded at time of collection (October 20-21, 2024). DBH measurements are the average DBH of each measurement taken at the sample point. Bolded values represent cores for which there is corresponding digital band dendrometer data. Explanation of site ID abbreviations: "DT" = "Discovery Trail"; "HQSWP" = "Headquarters Swamp"; "HQRIP" = "Headquarters Riparian".

After collection, each core was stored in a plastic or paper straw, then transferred to the OSU tree-ring lab to be glued to a mount and sanded. A Regent LA2400 scanner was used to acquire high-resolution images of the cores in WinDENDRO (Regent Instruments Inc.). WinDENDRO allowed us to measure total annual ring width, earlywood and latewood width, and wood density. Earlywood and latewood measurements, as well as latewood width and density measurements, together provide useful proxies for reconstructing past climate and tree responses to stress (Meko & Baisan, 2001; Campbell et al., 2011).

Images from WinDENDRO were uploaded into CooRecorder version 9.8.1 (Larsson, 2005) where annual boundaries for total ring-widths, earlywood & latewood, and blue light reflectance bands were automatically detected and manually checked. Each boundary was recorded in CooRecorder as a coordinate. Coordinate files were cross-dated and converted to ring-width measurements (mm) in CDENDRO version 9.8.1. The chronological accuracy of the cross-dating was validated with the program COFECHA (Holmes et al., 1986). After validation, ring-width measurements were converted to BAI (cm^2) using the bai.out function in the R package, "dplR" (Bunn, 2010; Bunn et al., 2025).

2.7 Statistical Modeling

Statistical models are useful in forest ecology to help reduce uncertainty related to the many confounding genetic and environmental variables that influence tree growth (Rupsys et al., 2010). In the present study, such models allow for clearer interpretations and predictions of potential population-level effects despite our small sample size.

2.7.1 Gompertz Models

Standard and first derivatives of Gompertz deterministic growth models were fitted using the dm.fit.gompertz function in DendRoAnalyst, which summarizes data to a daily resolution. This first required the removal or interpolation of any missing or "NA" values. DendRoAnalyst has a function to interpolate data gaps, but we did not use this due to the extended duration of data gaps. We estimated the date of maximum growth rate for each tree and year by identifying the date when the first derivative Gompertz curve reached its maximum value. We estimated the start and end of the GS for each tree and each year based on methods detailed in Li et al. (2022), where the dates at which the 5% and 95% of the total annual modeled growth from standard Gompertz curves correspond to the start and end of the growing season, respectively (Li et al., 2022). The accuracy of these estimates were assessed by visually inspecting plots based on DendRoAnalyst's phase.sc function, which uses the Stem-cycle growth approach to define each day as representing stem shrinkage, expansion, or permanent increment (Deslauriers et al., 2011; Downes et al., 1999). Obtaining this information allowed us to more confidently and accurately calculate expansion metrics without the interference of confounding variables such as autumnal rain expansion.

2.7.2 Linear mixed effects model

To disentangle natural variation driven by year, specific tree, and phenology, we fitted a linear mixed effects model (Laird & Ware, 1982). To minimize diurnal and seasonality effects while capturing immediate and short-term impacts, our model uses daily BAI data from a truncated calendar window that starts 2 weeks before the Heat Dome's onset and ends 2 weeks after the Heat Dome's conclusion (June 12-July 12).

We categorized these calendar dates into three periods based on their temporal proximity to the dates of the Heat Dome: “before” (June 12-25), “during” (June 26-28), and “after” (June 29-July 12). This allowed us to compare changes in expansion during the same calendar dates across all years, which helps in accounting for seasonal phenology. The years included in the model range from two years before the Heat Dome to two years after the Heat Dome (2019-2023).

Our model only includes the 6 Douglas-firs on which an electronic band dendrometer was installed at breast height. We omitted the remaining 5 trees because their dendrometer position, species, and/or installation dates did not have enough replicates to include. Of the six included trees, two are old-growth (IDs 310, 311), and four are second-growth (IDs 654, 655, 656, 860). These two age classes are acknowledged in the model as added fixed effects to account for the different growth responses that arise from trees that are vastly different ages and sizes. Given this limited sample size, the model tests the effects of age class by itself but does not test the effects of age class interacting with the other two fixed effects. The ID of each individual is treated as a random effect in our model to account for individual tree variation without explicitly testing for tree-level effects. Tree ID 860 experienced severe canopy damage due to an ice storm in early 2024, so only data from 2019-2023 are included for that tree.

Our model equation incorporating the variables explained above is detailed below. The model statement and effects for the model are summarized in **Table 4**. We used age class, year, period, and the interaction of year and period as fixed effects, and individual tree ID as a random effect. We assessed model assumptions of normal and identically distributed errors by visually inspecting residual plots. We also checked for temporal autocorrelation of sequential expansion/contraction increments within trees by visually inspecting autocorrelation function (ACF) plots. We used the common threshold $\alpha = 0.05$ for identifying deviations from assumptions.

$$y_{ijkl} = \mu + \alpha_i + \beta_j + (\alpha\beta)_{ij} + \gamma_k + u_l + \varepsilon_{ijkl}$$

where μ is the overall mean response, α_i is the effect of period i, β_j

is the effect of year j

, γ_k

is the effect of age class k

, and $u_1, u_2, \ldots, u_L \sim N\left(0, \sigma_u^2\right)$

are random effects for the individual tree.

BAI ~ Year * Period + AgeClass + (1 | ID)		
Variable	**Effect**	**N Factor Levels (Levels)**
AgeClass	Fixed	**2** ("SecondGrowth", "OldGrowth")
Period	Fixed	**3** ("before", "during", "after")
Year	Fixed	**7** ("2019", "2020", "2021", "2022", "2023", "2024", "2025")
ID	Random	**6** ("310", "311", "654", "655", "656", "860")

Table 4: Summary of variable attributes used in our linear mixed-effects model.

To answer specific questions about Heat Dome impacts, we used the R package "emmeans" version 1.11 to create custom contrasts and calculate estimated marginal means (EMMs) with "multivariate-t" adjustment (Lenth, 2025). These EMMs represent marginal averages from our linear model. One goal of setting custom EMM contrasts is to explicitly test if the difference in BAI during versus before the Heat Dome period ("during" – "before") significantly varies across three time periods: two years before the Heat Dome (2019-2020), the year of the Heat Dome (2021), and the two years after the Heat Dome (2022-2023). This should convey conditions before the Heat Dome, immediate Heat Dome effects, and next GS carryover effects. The "before" period is included to still account for seasonal phenological variability within each tree and year group. This process was repeated for "after" – "before" differences to distinguish how the Heat Dome affected growth during the remainder of the GS relative to before the event. By comparing annual differences ("during" – "before" and "after" – "before") rather than "during" and "after" periods by themselves, we control for inter-annual variation and ensure that each year is compared to its own baseline ("before") condition. Our discussion will prioritize results of these contrasts.

The Heat Dome occurred at a time when growth rates are typically starting to decline for the GS, so an interaction term of year*period was added to explicitly test whether the effects of the Heat Dome were different in 2021 compared to the same

time period in other years. This test was done with the interaction term of year*period. We included the interaction between year and period to estimate the deviation of mean growth during and after the heat dome from the mean during the same periods in the season but in years prior to 2021. Because we fitted the model with “nlme” version 3.1-166, the model was reparameterized internally using the ‘regression parameterization’, also known as ‘dummy coding’. The baseline level was defined as second-growth trees in the before period of 2019.

3.0 Results

3.1 Trends and observations in microclimate (RQ2)

To determine whether the trends observed above can be elucidated by microclimate patterns, we first viewed the data at its finest temporal resolution on two important timescales: the full data range as well as the two-month window in which the Heat Dome occurred. **Figures 3-6** display upper-canopy air temperature, upper-canopy VPD, daily rainfall, and HDI respectively. These figures include dates corresponding to three wildfires taking place at the HJA during the record: the Holiday Farm Fire (September 7 - October October 16, 2020); the Lookout Fire (August 7 - September 29, 2023); and the Ore Fire (July 16 - September 16, 2024). The Lookout Fire caused a data gap for VPD, air temperature, and precipitation ranging from September 15-28, 2020.

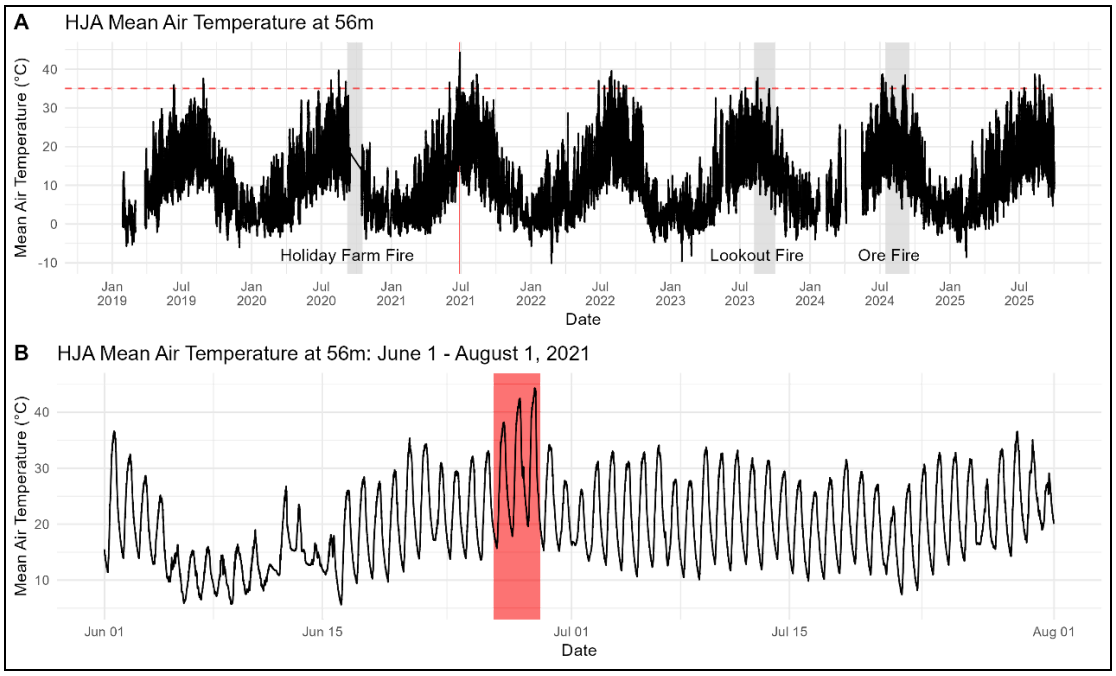

Figure 3: Full record of mean 5-minute high-resolution upper-canopy air temperature (A) and mean high-resolution upper-canopy air temperature spanning from June 1 – August 1, 2021 (B). Red horizontal dashed line (A) indicates the stress threshold for SDH. Red vertical bars correspond to the dates of the Heat Dome (June 26-28). Gray vertical bars (A) indicate the dates of three fires occurring during the record.

Locally, the Heat Dome was most severe June 26-28. Mean air temperature on the latter two days exceeded 40°C for multiple hours, after which mean air temperature remained high throughout the entirety of summer (**Figure 3**).The temperature, VPD, and HDI peaks associated with the Heat Dome were the highest within the entire time record (**Figure 4**). Strong similarities between VPD and HDI are expected since VPD drives HDI.

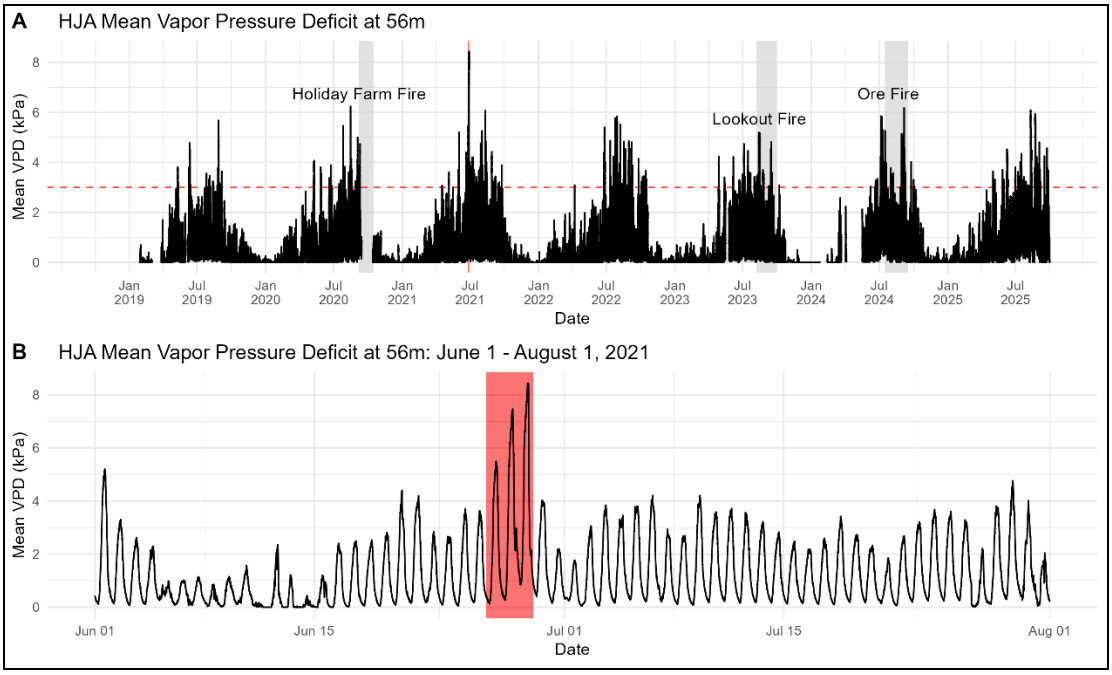

Figure 4: Full record of mean high-resolution upper-canopy VPD (A) and mean high-resolution upper-canopy VPD spanning from June 1 – August 1, 2021 (B). Red horizontal dashed line (A) indicates the stress threshold for SVH.Red vertical bars correspond to the dates of the Heat Dome (June 26-28). Gray vertical bars (A) indicate the dates of three fires occurring during the record.

Singular rain events in the 2020 water year were frequent but small. The following year, there was abundant rainfall in the first half of the 2021 water year (**Figure 5**). Moreover, there were nine days in the month leading up to the Heat Dome in which rainfall occurred (**Figure 5**), although only four days exceeded 0.1 cm. The onset of the Heat Dome was preceded by ten consecutive days of no rainfall. In the month following the Heat Dome, there were two days of rainfall, one of which exceeded 0.1 cm. The first of these two rain events took place 30 days after the onset of the Heat Dome.

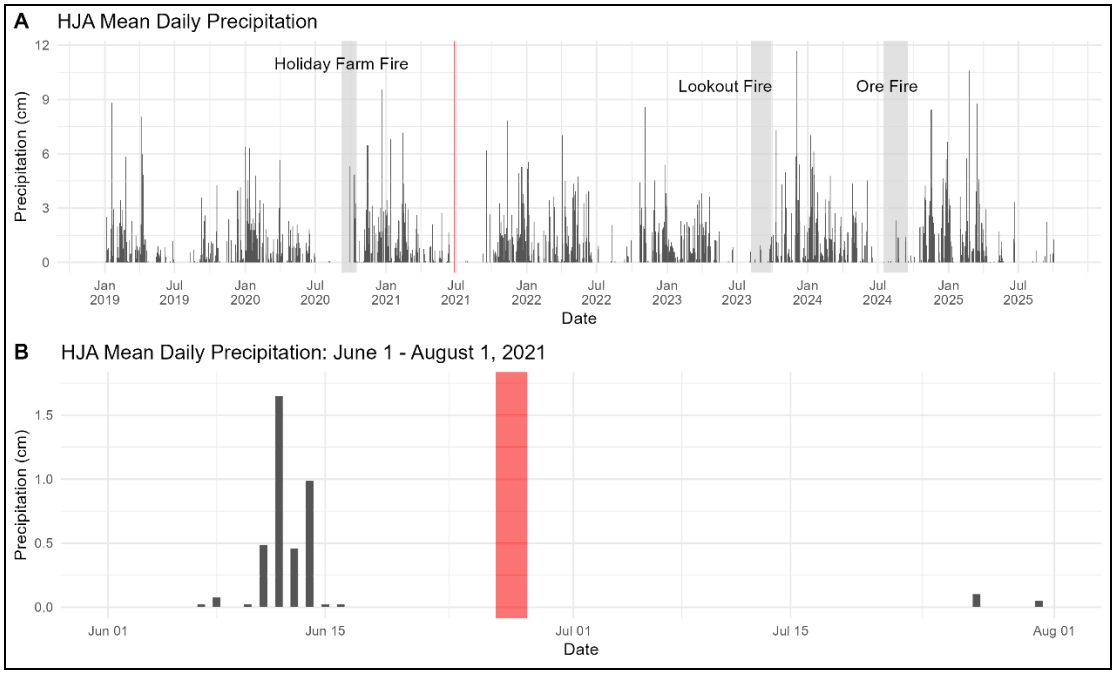

Figure 5: Full record of mean daily precipitation (A) and mean daily precipitation spanning from June 1 – August 1, 2021 (B). Red vertical bars correspond to the dates of the Heat Dome (June 26-28). Gray vertical bars (A) indicate the dates of three fires occurring during the record.

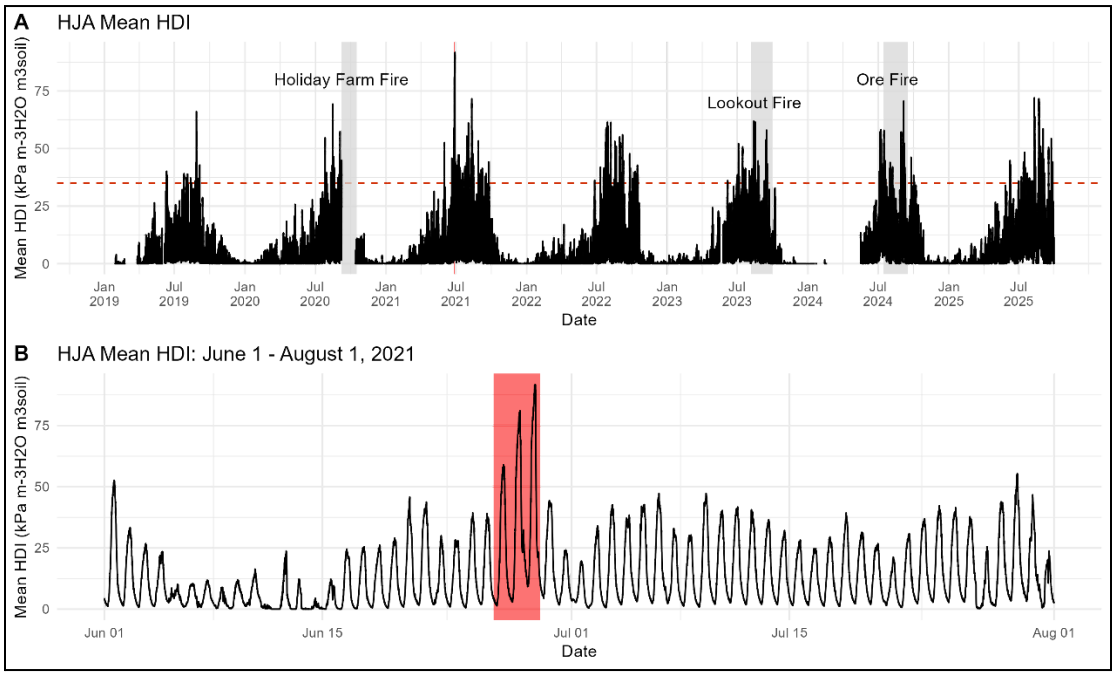

Figure 6: Full record of mean HDI (A) and mean HDI spanning from June 1 – August 1, 2021 (B). Red horizontal dashed line (A) indicates the stress threshold for SHH. Red vertical bars correspond to the dates of the Heat Dome (June 26-28). Gray vertical bars (A) indicate the dates of three fires occurring during the record.

Annual cumulative statistics for SDH, SVH, and SHH, are shown in **Figures 7-9** and summarized alongside precipitation in **Tables 5-6**. Data end at the conclusion of the 2025 water year. To reflect these water year scales, **Table 6** ranges from January to October. We can infer that the ranking of 2025 will not change as it is unlikely that there will be a significant accumulation of metrics that surpass our stress thresholds in the autumn and winter months. 2021 was undoubtedly the most stressful year in our high-frequency record for all three cumulative stress metrics, mostly in terms of SDH. SDH in the 2021 GS was almost double that of the second-highest accumulated SDH, occurring in 2022. 2022 also had the second-highest accumulated SVH (**Figure 8**).

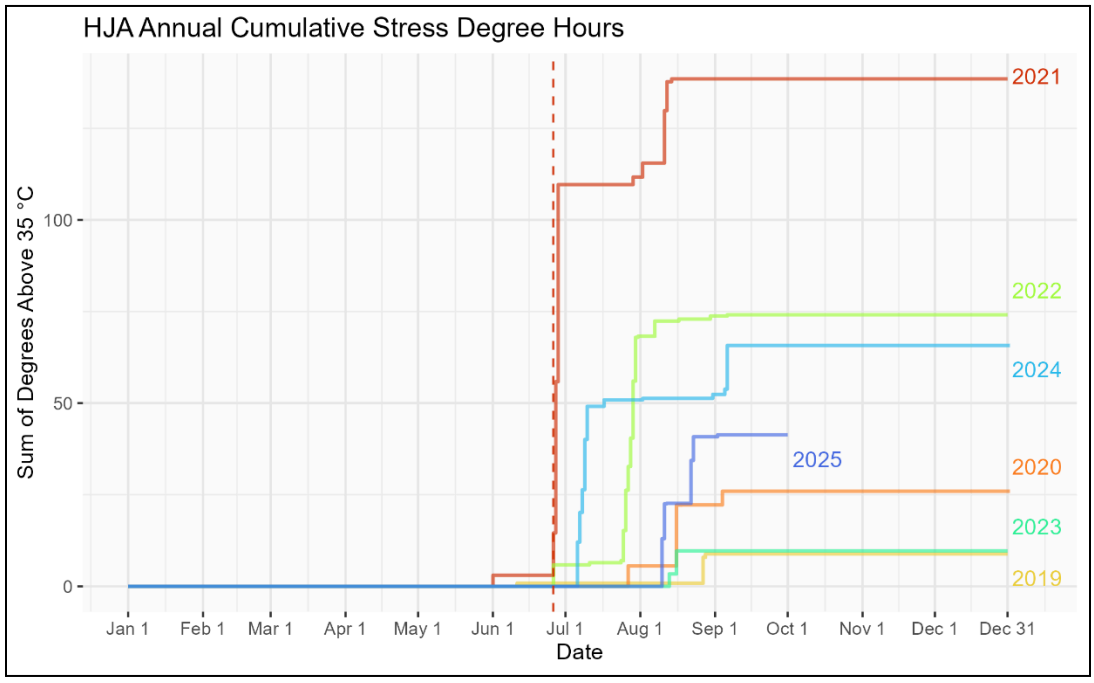

Figure 7: Annual accumulation of hourly degrees above 35°C. Red vertical dashed line indicates onset of Heat Dome (June 26).

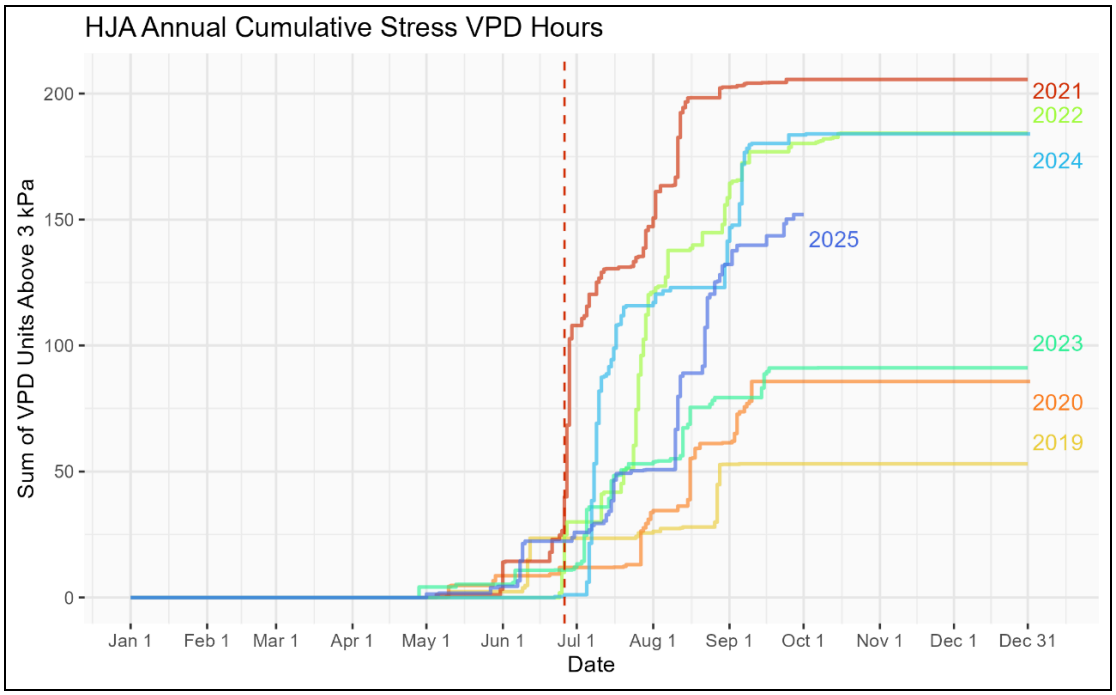

Figure 8: Annual accumulation of hourly VPD values above 3 kPa. Red vertical dashed line indicates onset of Heat Dome (June 26).

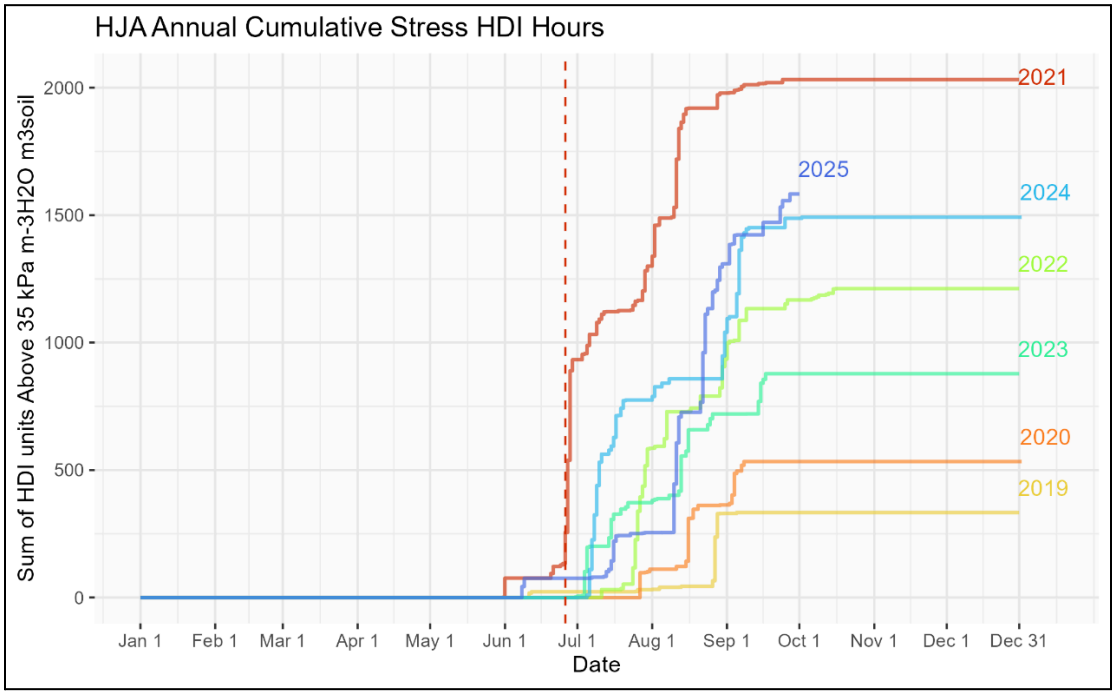

Figure 9: Annual accumulation of hourly HDI values above 35 kPa $m^{-3}H_20$ m^3soil. Red vertical dashed line indicates onset of Heat Dome (June 26).

Cumulative precipitation is shown on two time scales in **Figure 10**: complete water years (panel A) and each year's GS plus March (panel B) to observe potential

influences of spring rains. The 2023 water year had the least total precipitation in our high-frequency record, and 2024 had the most (**Figure 10**). Although the 2023 water year was driest overall, it had the second highest accumulated rainfall during the 2023 GS and its preceding spring. 2021 exhibits an opposite pattern; the total 2021 water year yielded an intermediate amount of rain, but precipitation strictly within the 2021 GS was far below that of the other years. 2022 had the wettest spring and summer by a considerable margin (47.02 cm) (**Table 6**).

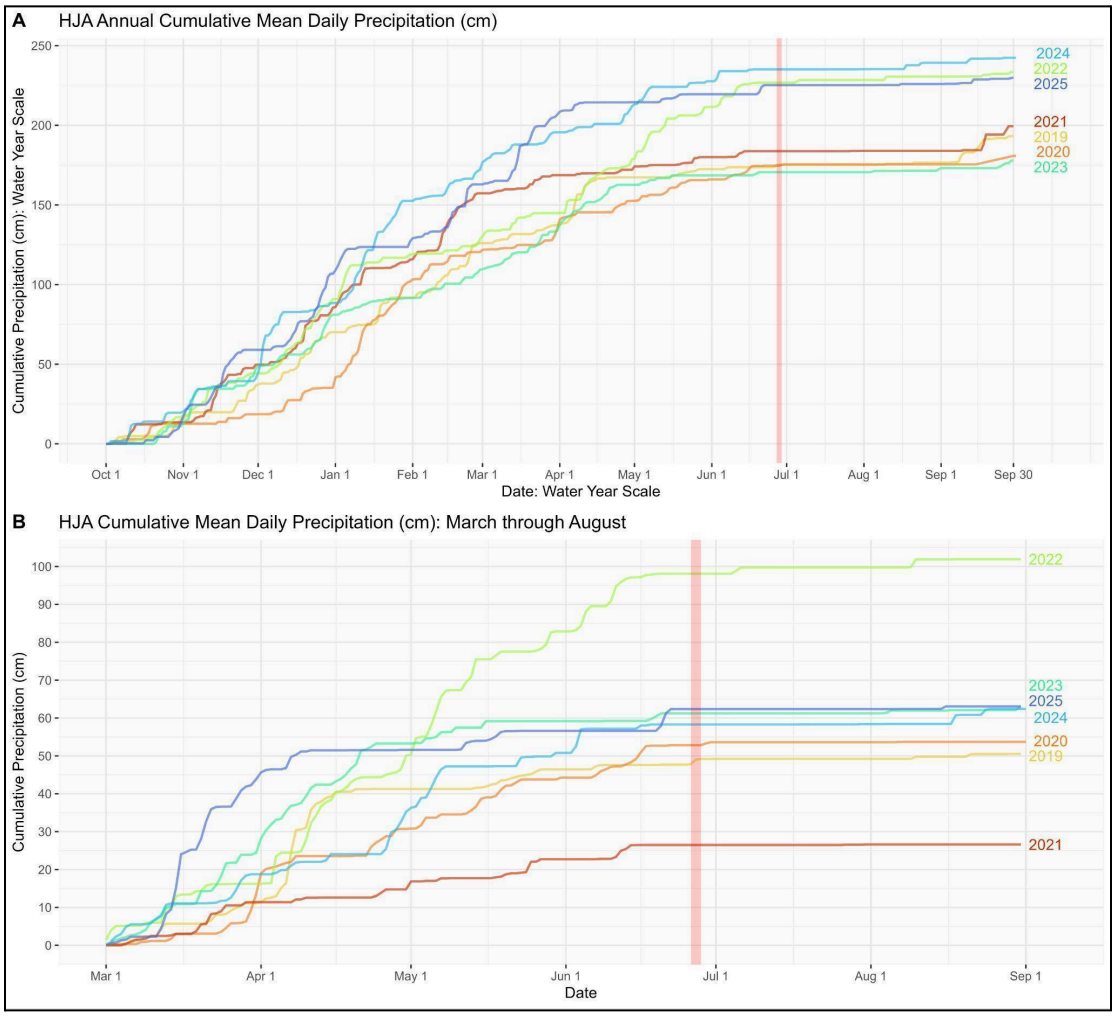

Figure 10: Annual accumulation of precipitation in cm. Red vertical dashed line indicates onset of Heat Dome (June 26).

	Cumulative Microclimate Metrics (April through August)			
Year	**Precipitation (cm)**	**SHH (kPa $m^{-3}H_2O$ m^3soil-hours)**	**SDH (°C-hours)**	**SVH (kPa-hours)**
2019	39.4	329.87	8.84	52.83

2020	34.67	363.19	22.23	61.4
2021	15.24	1978.78	138.52	202.53
2022	85.7	905.45	73.77	155.79
2023	38.68	720.23	9.67	79.39
2024	43.66	1040.28	52.38	141.36
2025	19.25	1308.67	40.84	132.17

Table 5: Cumulative precipitation (cm), stress HDI hours (kPa m-3H2O m3soil-hours), stress degree hours (°C-hours), and stress VPD hours (kPA-hours) spanning the approximate GS (April through August). Cells shaded red denote the most stressful value for that year (lowest precipitation or highest stress metric), whereas cells shaded cyan denote the least stressful value for that year (highest precipitation or lowest stress metric).

	Cumulative Microclimate Metrics (January through September*)			
Year	**Precipitation (cm)**	**SHH (kPa $m^{-3}H_2O$ m^3soil-hours)**	**SDH (°C-hours)**	**SVH (kPa-hours)**
2019	123.32	333.05	8.84	53.08
2020	145.54	533.21	25.96	85.73
2021	113.92	2032.44	138.52	205.63
2022	142.65	1167.45	74.11	180.21
2023	96.98	877.98	9.67	91.08
2024	154	1487.88	65.75	183.6
2025	123.22	1583.02	41.36	152.02

Table 6: Cumulative precipitation (cm), stress HDI hours (kPa m-3H2O m3soil-hours), stress degree hours (°C-hours), and stress VPD hours (kPA-hours) spanning January through September. Cells shaded red denote the most stressful value for that year (lowest precipitation or highest stress metric), whereas cells shaded cyan denote the least stressful value for that year (highest precipitation or lowest stress metric). "" indicates a data gap for this year.*

3.2 Trends and observations in high-resolution tree growth (RQ1)

3.2.1 Observations and comparisons of growing seasons

Figure 11 shows the start, end, and duration of the estimated GS for each year and tree in the below-canopy digital band dendrometer record. These data are summarized in **Table 7**. ID 309 is excluded as its unusual expansion-contraction patterns in the mid canopy led to inaccurate estimates of the GS.

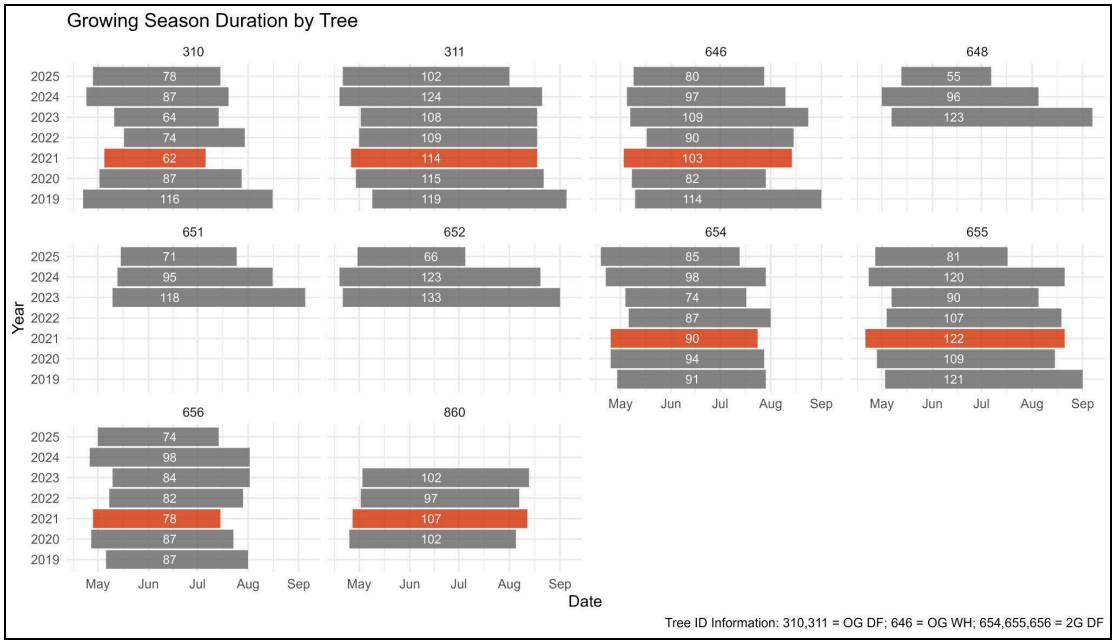

Figure 11: GS metrics for each tree and tree for which a digital band dendrometer is installed on the lower bole. Vertical bars correspond to the Heat Dome timing. Growing season metrics for 2021 are shaded red. Text inside each bar corresponds to the duration (in number of days) of the GS for that year. Instrumented trees include three Old-Growth Douglas-firs (tree IDs 309, 310, 311), four second-growth Douglas-firs (tree IDs 654, 655, 656, 860), three old-growth western hemlocks (tree IDs 646, 648, 652), and one old-growth western red cedar (tree ID 651).

The average GS ranged from May 2 to August 6, with expansion rates peaking around May 29 for most trees. Few observations deviate from this general trend. Most notably, ID 310 (OG DF) ceased increment growth approximately one week after the Heat Dome (July 6), marking the earliest end to a GS for this tree and the second earliest end to a GS across all trees and years studied. For the same tree, 2021 also had the shortest GS at 62 days, marking the shortest total GS across all trees and years. The shortest total GS lasted 55 days in 2025 for ID 648 (OG WH), although there is a shorter data record for this tree compared to others; he earliest GS end date occurred for ID 652 (OG WH) on July 5, 2025, just a day later than the GS end date for IG 310 in 2021. Conversely, some individual trees (had GS lengths in 2019 and 2023 that extended beyond the expected early August norm, going into September. Since these instances are relatively isolated, GS analyses hereafter will focus on a window of April through August.

On average across all trees with a dendrometer installed at breast height, the 2021 GS was 29 days shorter than the other years within our 2019-2025 record.

resulted in a few other minimum or maximum values for different metrics. Similarly to tree ID 310, Tree ID 656 (2G DF) stopped adding BAI on July 15, 2021. Two of the six trees with the full 7-year record had their earliest GS start date in 2021. One was an OG WH (ID 646), and the other was a 2G DF (ID 655), which had its longest GS in 2021. When adding the GS duration of all trees together, 2025 had the fewest combined GS days, followed by 2023, 2022, then 2021 (**Figure 12**).

	Old growth Douglas-fir		Old growth western hemlock			OG WRC	2nd growth Douglas-fir			
	310	311	646	648†	652†	651†	654	655	656	860††
Earliest GS Start	April 22, 2019	April 18, 2024	May 3, 2021	April 30, 2024	April 18, 2024	May 10, 2023	April 19, 2025	April 21, 2021	April 25, 2024	April 24, 2020
Latest GS Start	May 17, 2022	May 9, 2019	May 17, 2022	May 13, 2025	April 30, 2025	May 15, 2025	May 6, 2022	May 7, 2023	May 10, 2023	May 3, 2023
Earliest GS End	July 6, 2021	Aug. 1, 2025	July 28, 2020 2025	July 7, 2025	July 5, 2025	July 25, 2025	July 13, 2025	July 17, 2025	July 14, 2025	Aug. 4, 2020
Latest GS End	Aug. 16, 2019	Sep. 5, 2019	Sept. 1, 2022	Sep. 7, 2023	Sep, 1, 2023	Sep. 5, 2023	Aug. 1, 2022	Sept. 1, 2019	Aug. 2, 2023	Aug 13, 2023
Shortest GS (n days)	62	102	80	55	66	71	74	81	74	97
Year of Shortest GS	2021	2025	2025	2025	2025	2025	2023	2025	2025	2022
Longest GS (n days)	116	124	114	123	133	118	98	122	98	107
Length of 2021 GS - Length of Avg. GS	-19.14	1	6.57	-91.33	-94.67	-107.33	1.57	14.86	-6.29	5
Year of Longest GS	2019	2024	2019	2023	2023	2023	2024	2021	2024	2021
Earliest Max Expansion Rate Date	May 17, 2024	May 19, 2025	May 29, 2020	May 26, 2024	May 18, 2025	June 3, 2025	May 12, 2025	May 19, 2025	May 19, 2021	May 22, 2020
Latest Max Expansion Rate Date	June 6, 2022	June 17, 2019	June 15, 2019	June 17, 2023	June 1, 2023	June 18, 2023	May 30, 2022	June 10, 2019	June 2, 2023	June 1, 2023
Year of least	2025	2019	2024	2025	2025	2025	2019	2019	2019	2023

expansion										
Year of most expansion	2020	2020	2021	2024	2024	2024	2022	2020	2020	2020

Table 7: Maxima and minima of GS metrics for each tree. Columns shaded in light gray do not have the full 7-year data record to accurately compare with other columns. "†" indicates that the available record for this column spans from 2023-2025, whereas "††" indicates that the available record for this column spans from 2020-2023. Cells shaded red denote values that occurred in 2021. If there was a tie for a value, both years are included. "OG WRC" refers to old growth western redcedar.

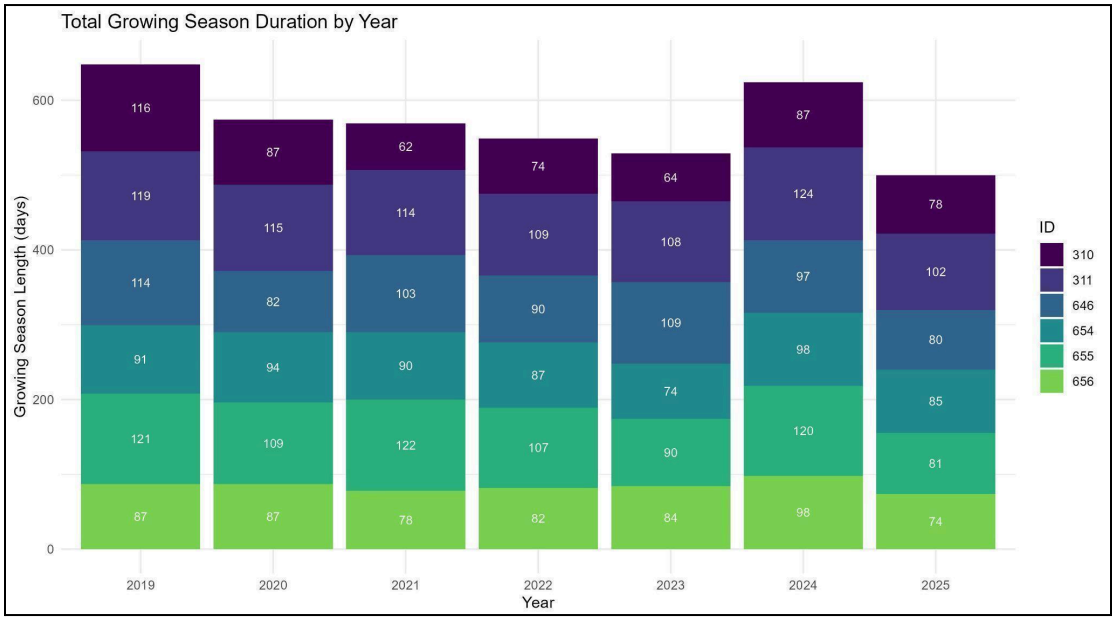

Figure 12: GS duration (in number of days) combined across all trees per year. From shortest to longest, the order of combined GS days is as follows: 2025, 2023, 2022, 2021, 2020, 2023, 2019. Trees include two Old-Growth Douglas-firs (tree IDs 310, 311), three second-growth Douglas-firs (tree IDs 654, 655, 656), and one old-growth western hemlocks (tree ID 646).

3.2.2 Observations and comparisons of BAI

Figure 13 shows stem expansion curves for IDs 310 (OG DF) and 656 (2G DF) over the approximate GS (April through August) for 2020 and 2021. 2020 was chosen for comparison due to the high increment added during this year. Standardized modeled growth rate, HDI, and precipitation are added to observe how these metrics interact to influence growth.

Rain events in the 2020 GS were small but numerous, whereas rain events in the 2021 GS were small *and* infrequent. Across both years, both trees expand at similar rates until they reach a similar date of maximum expansion (**Figure 13, Table 7**). The narrow modeled growth rate curves for both trees in 2021 compared to 2020 indicate that growth rates quickly declined after peaking. In terms of observed BAI,

ID 656 shows similar patterns of cumulative BAI in 2020 and 2021; the only noteworthy difference is the negative increment occurring in direct response to the Heat Dome as evidenced by the concurrent spike in HDI, an event that the tree seemingly recovers from rather quickly even as HDI remains high for the remainder of the GS. For ID 310, however, stem contraction from Heat Dome is much more severe, and it does not recover for the remainder of the GS. Small bumps in the growth curve in August likely correspond to small rain events that occur during the same time.

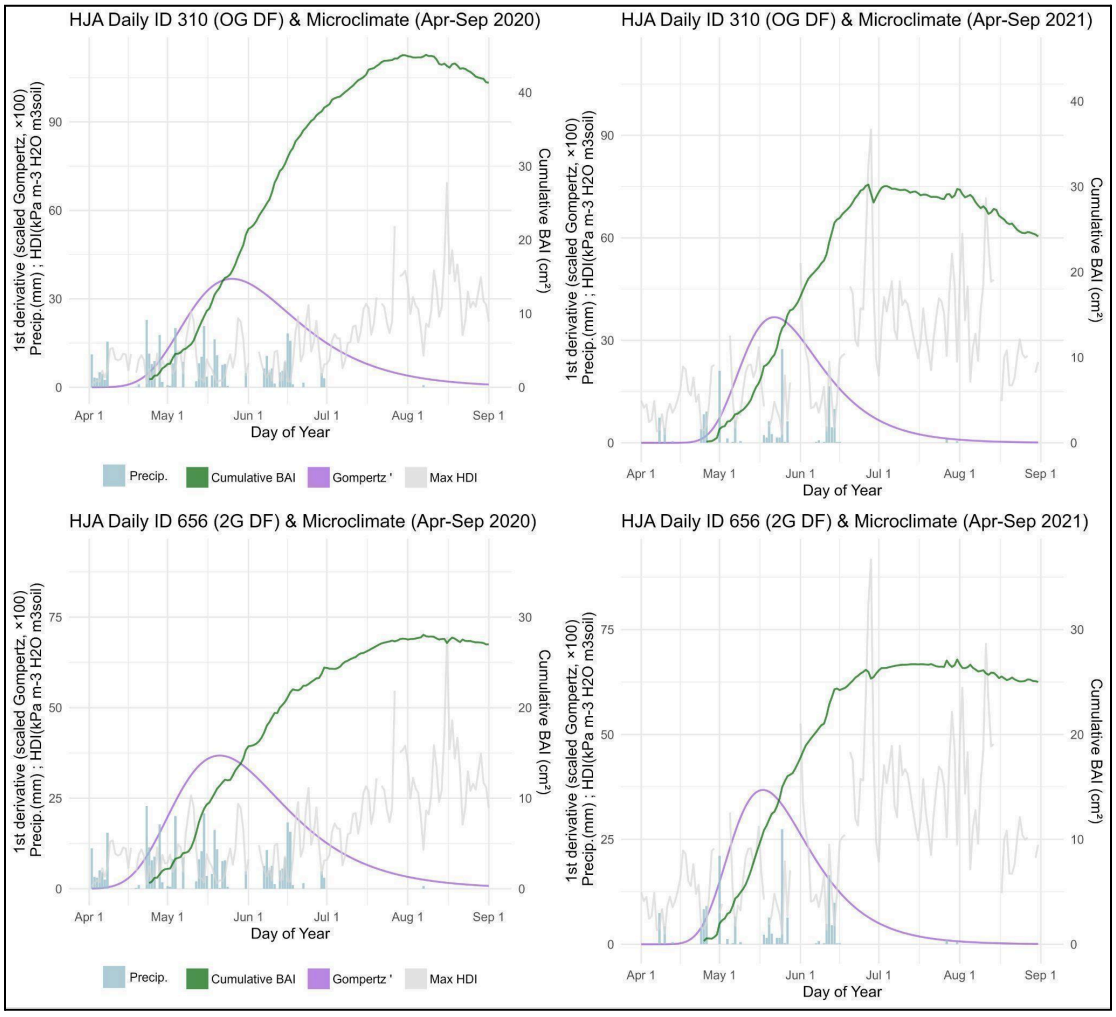

Figure 13: Plots of cumulative BAI (cm^2), precipitation (cm), standardized Gompertz growth rate, and HDI (kPa m-3H2O m3soil) for IDs 310 (OG DF) and 656 (2G DF) during the approximate GS (April through August) of 2020 and 2021.

Figure 14 shows the result of summarizing raw dendrometer increment data (**Figure 2**) to daily resolution and then converting to cumulative BAI (cm^2) with cyclic stem expansion phases identified. As mentioned, tree ID 860 (second-growth DF) exhibits little to no increment after 2023 as its canopy was heavily damaged by a winter ice storm that occurred in early 2024 The expansion pattern of Tree ID 309 (mid canopy OG DF) also deviates from the others, as its dendrometer is the only one installed above breast height.

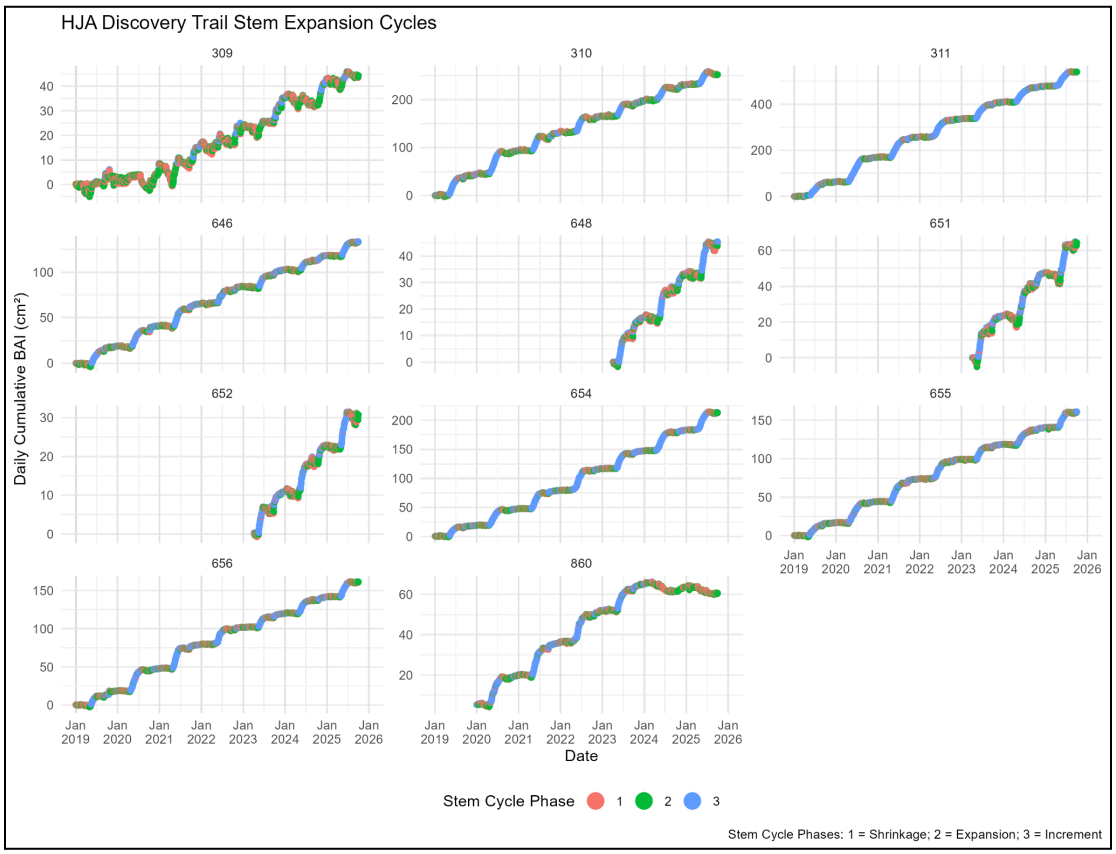

Figure 14: Plots of raw dendrometer data (Figure 2) converted to cumulative daily BAI (cm^2). Colors within each plot correspond to stem phases identified via dendRoAnalyst. Instrumented trees include three Old-Growth Douglas-firs (tree IDs 309, 310, 311), four second-growth Douglas-firs (tree IDs 654, 655, 656, 860), three old-growth western hemlocks (tree IDs 646, 648, 652), and one old-growth western red cedar (tree ID 651).

To highlight Heat Dome impacts in 2021, **Figure 15** shows the same data as **Figure 14** but truncated to highlight changes in cumulative BAI 2 weeks before and after the Heat Dome. Aside from ID 309, which is measuring different responses than the other trees given its in-canopy placement, ID 310 (OG DF) had the most severe immediate response to the Heat Dome,: its cross-sectional area temporarily shrank by

1.26 cm² from the onset of the Heat Dome (June 26) to its conclusion (June 28) due to water loss (**Table 8**). ID 310 is the second-largest tree in our sample (Table 3) and it is the only sample tree that fails to put on positive increment for the remainder of the 2021. All other trees (IDs 646 [OG WH], 654, 655, and 656 [2G DF]) begin expanding again starting June 29 and resume positive increment growth by July 2 at the latest, signaling at least some degree of short-term recovery (**Figure 15, Table 8**). ID 311 (OG DF), was the only sample tree that continued to have positive increment growth in the immediate aftermath of the Heat Dome. Tree IDs 310 and 311 (OG DF) are the only trees to show a 1-day lagged response to the Heat Dome, as indicated by their positive increment on the second day of the event (June 27).

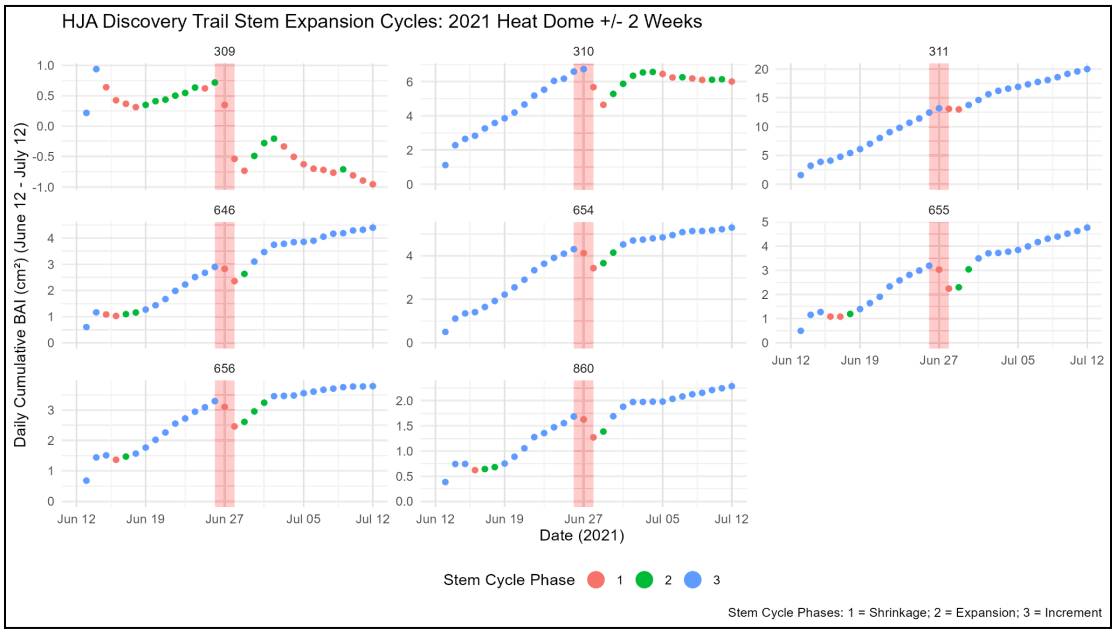

Figure 15: Plots of daily cumulative BAI (cm²) two weeks before and after the Heat Dome (June 12 - July 12, 2021). Colors within each plot correspond to stem phases identified via dendRoAnalyst. Shaded red region corresponds to the dates of the Heat Dome at the Andrews Forest (June 26-28). Instrumented trees include three Old growth Douglas-firs (tree IDs 309 [canopy], 310, 311), four second-growth Douglas-firs (tree IDs 654, 655, 656, 860), and one old-growth western hemlock (tree ID 646).

ID	ΔCumu. BAI June 26-28 (cm²)	ΔCumu. BAI June 26 - July 2 (cm²)
309	-1.26	-0.92
310	-0.91	-0.24
311	**0.65**	**3.20**
646	-0.54	**0.85**
654	-0.87	**0.40**
655	-0.95	**0.52**
656	-0.83	**0.16**

860	-0.42	**0.29**

*Table 8: Table demonstrating the change in cumulative BAI (cm^2) on two time scales:the start of the Heat Dome versus the end of the Heat Dome (June 26-28) as well as the start of the Heat Dome versus the day after the end of the Heat Dome (June 26-29). **Bold** values indicate positive increment. Instrumented trees include three Old-Growth Douglas-firs (tree IDs 309, 310, 311), four second-growth Douglas-firs (tree IDs 654, 655, 656, 860), and one old-growth western hemlock (tree ID 646).*

Figure 16 shows annual stem expansion curves for the approximate GS of all sample trees across the complete time record available at its highest resolution. Only the GS (April 1- August 31) is shown to highlight true expansion from growth and not bark swell from autumnal rain. Just as in **Figures 14-15**, mid-canopy measurements from ID 309 are uniquely variable and unstable compared to the measurements taken at breast height. All trees except two with full 7-year records added the most increment during the 2020 GS (**Table 9**). ID 654 (2G DF) added the most during the 2022 GS, and ID 646 (OG WH) added the most during the 2021 GS. Similarly, all except two trees with the full 7-year record added the least increment during the 2019 GS (**Table 9**). ID 310 (OG DF) added the least during the 2025 GS, and ID 646 (OG WH) added the least during the 2022 GS. The year with the longest cumulative GS days across all trees (2019; **Figure 12**) also had the most trees with their slowest growth year in the dendrometer record, which is relatively short (**Table 7, 9**).

Figure 7 highlights the fact that ID 310 (OG DF) had the most severe response to the Heat Dome impacts and is the only sample tree that does not add any increment for the remainder of the GS, although the positive increment of ID 656 (2G DF) is minimal during the same time period. Annual increment after 2021 is somewhat inconsistent across trees, but 2023-2025 tend to be among the poorer years for annual increment growth. The effects of ice damage on ID 860 (2G DF) are clearly seen as negative increments in 2024 and 2025 after the corresponding storm took place.

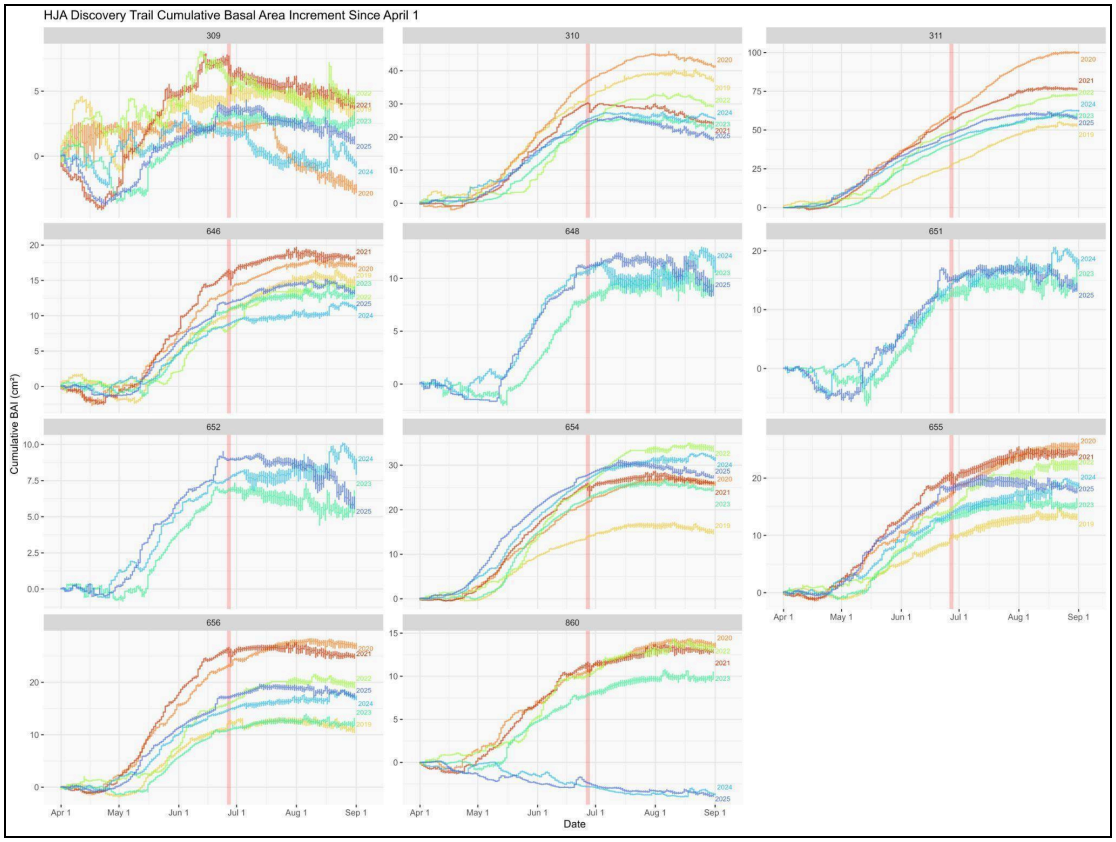

Figure 16: Plots of cumulative BAI (cm^2) during the approximate GS (April 1 through August 31) for each dendrometer and each year. Red vertical bars correspond to the dates of the Heat Dome (June 26-28, 2021), and the 2021 GS is shown in dark red. Instrumented trees include three Old-Growth Douglas-firs (tree IDs 309, 310, 311), four second-growth Douglas-firs (tree IDs 654, 655, 656, 860), three old-growth western hemlocks (tree IDs 646, 648, 652), and one old-growth western red cedar (tree ID 651).

Figure 17 shows the same GS data for DF trees from different age classes: old-growth (IDs 310, 311) and second-growth (IDs 655, 656). The fluctuation in the shape of each line represents diurnal stem fluctuations that are captured by the dendrometers at 5-minute increments. This figure highlights the role of tree size and age; the two OG trees, for example, have delayed contraction responses to the Heat Dome whereas the two 2G trees shrink almost immediately as the Heat Dome begins.

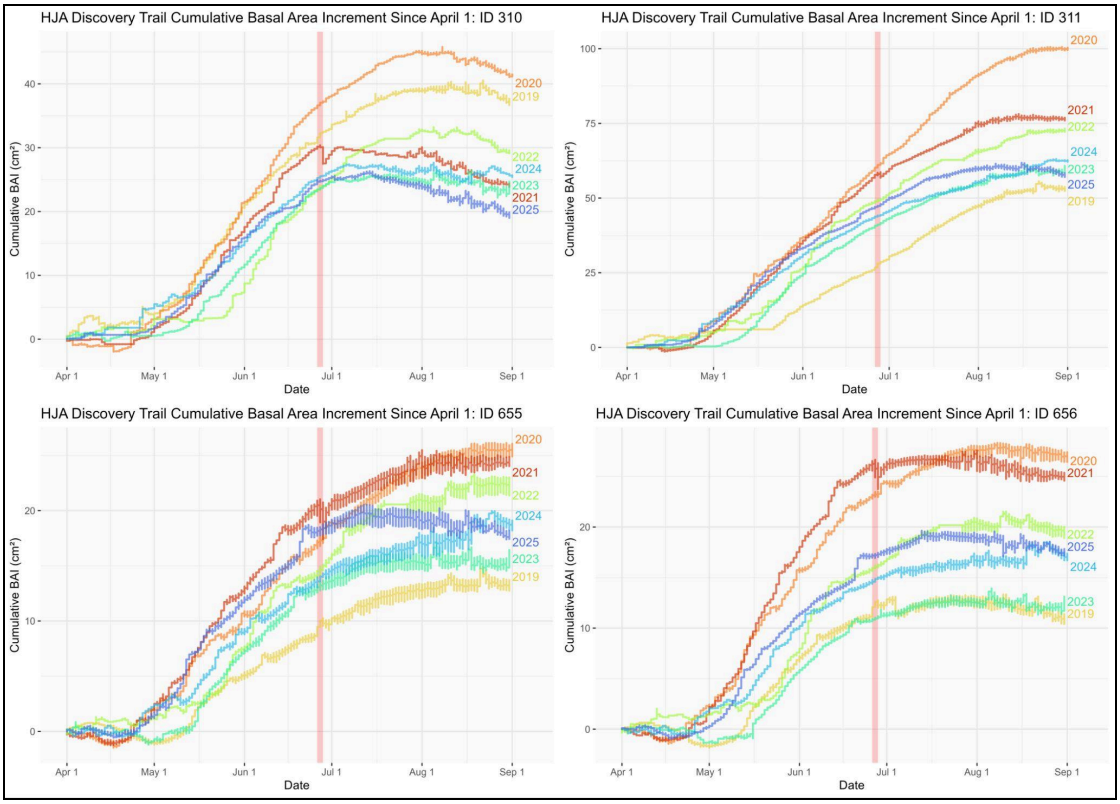

Figure 17: Plots of cumulative BAI (cm^2) during the approximate GS (April through August) for each year of IDs 310,311,655, and 656. Red vertical bars correspond to the dates of the Heat Dome (June 26-28).

Total stem basal area increment (cm^2): April through August

	OG DF		OG WH	2nd-growth DF		
Year	**310**	**311**	**646**	**654**	**655**	**656**
2019	36.88	52.98	14.8	14.92	13.17	10.82
2020	41.31	100.02	17.23	25.95	25.62	27.08
2021	23.88	76.31	18.13	25.91	24.32	24.85
2022	29.14	72.46	13.84	33.73	22.26	19.5
2023	24.85	60.87	14.09	25.4	16.52	13.2
2024	25.4	62.39	11.03	31.25	18.71	17.01
2025	19.35	57.71	13.28	27.19	17.66	17.42

Table 9: BAI (cm^2) ranging from April through August for sample trees with the full 7-year record available. Cells shaded red denote the lowest value for that ID, whereas cells shaded cyan denote the highest value for that ID.

3.2.3 Results of the linear-mixed model

Table 10 shows the estimated differences in mean BAI from our linear mixed-effects model to explicitly test Heat Dome impacts on Douglas-fir growth after accounting for inter-annual variability, intra-annual seasonality, and individual

variability within the six trees included in our model (IDs 310, 311 [OG DF], 654, 655, 656, 860 [2G DF]). BAI differences between different calendar periods are visualized in **Figure 18**, and the comparison of those BAI differences between year groups are visualized in **Figure 19**. As mentioned in our methods, investigating how the difference in BAI between calendar periods changes in each year group accounts for intra-annual variability in a way that cannot be fully achieved by comparing BAI during a certain period by itself.

During the Heat Dome (June 26-28, 2021), estimated mean BAI decreased by 0.82 cm^2/day (95% confidence interval [-0.96,-0.68] cm^2/day) compared to the average daily BAI in the 2 weeks preceding it (June 12-25, 2021). When comparing mean BAI between these same calendar date periods ("during" - "before") before 2021 (2019 and 2020), mean BAI was significantly greater in the "during" period by an estimate of 0.19 cm^2/day (95% confidence interval [0.093, 0.29] cm^2/day) (**Figure 18**), which is about 1 cm^2/day more than the same period difference ("during" - "before") in 2021 (95% confidence interval [0.81, 1.22] cm^2/day) (**Figure 19**). This increase of increment between calendar periods did not occur in the two years after 2021: in those years, BAI in the "during" period was not significantly different from BAI in the "before" period, although it is estimated that BAI is slightly lower in the "during" period in these years (95% confidence interval [–0.12, 0.079] cm^2/day).

In addition to comparing BAI estimates between "before" and "during" calendar periods, **Table 10** also shows results of statistical tests for short-term recovery after the Heat Dome and compares those results to other years. When comparing BAI in the two weeks *after* the calendar dates of the Heat Dome (June 26-28) to BAI in the 2 weeks preceding this period, mean increment declines in all years (**Figure 18**). However, this decline in increment from the "before" period to the "after" period is only significant during the Heat Dome year, when the decline is also the largest (95% confidence interval [–0.25, –0.082] cm^2/day). This decline from the "before" period to the "after" period in 2021 is 0.148 cm^2/day more severe than the increment decline in the two years afterward (95% confidence interval [–0.27, –0.027] cm^2/day) (**Table 10**) (**Figure 19**).

ΔBAI during - before the Heat Dome period							
Comparison Summary	**Comparison**	**Estimate**	**95% CI**	**T-ratio**	**df**	**P value**	**Result Summary**
Pre-HD year	2019-2020	0.19	0.093, 0.29	3.8	1214	0.0002	BAI ↑
HD year	2021	-0.82	–0.96, –0.68	-11.51	1214	<0.0001	BAI ↓
Post-HD year	2022-2023	-0.02	–0.12, 0.079	-0.39	1214	0.6968	BAI ↔
Pairwise comparisons of ΔBAI during - before the Heat Dome period							
Comparison Summary	**Comparison**	**Estimate**	**95% CI**	**T-ratio**	**df**	**P value**	**Result Summary**
Pre HD - HD years	2019-2020 versus 2021	1.01	0.81, 1.22	11.59	1214	<0.0001	BAI ↑↑
HD year - Post HD years	2021 versus 2022-2023	-0.80	–1.01, –0.60	-9.17	1214	<0.0001	BAI ↓↓
Pre HD years - Post HD years	2019-2020 versus 2022-2023	0.21	0.044, 0.38	2.96	1214	0.0088	BAI ↓
ΔBAI after - before the Heat Dome period							
Comparison Summary	**Comparison**	**Estimate**	**95% CI**	**T-ratio**	**df**	**P value**	**Result Summary**
Pre	2019-2020	-0.068	–0.13, –0.0092	-2.27	1214	0.0234	BAI ↓
HD	2021	-0.17	–0.25, –0.082	-3.90	1214	0.0001	BAI ↓
Post	2022-2023	-0.02	–0.076, 0.042	-0.56	1214	0.576	BAI ↔
Pairwise comparisons of ΔBAI after - before the Heat Dome period							
Comparison Summary	**Comparison**	**Estimate**	**95% CI**	**T-ratio**	**df**	**P value**	**Result Summary**
Pre - HD	2019-2020 versus 2021	0.097	–0.025, 0.22	1.87	1214	0.1479	BAI ↔
HD - Post	2021 versus 2022-2023	–0.148	–0.27, –0.027	-2.86	1214	0.0121	BAI ↓
Pre - Post	2019-2020 versus 2022-2023	–0.051	–0.15, 0.048	-1.21	1214	0.4477	BAI ↔

Table 10: Estimated marginal means for custom contrasts of modeled BAI (cm^2/day) ranging from June 12 - July 12 across 2019-2023 for 6 sample trees. "↑" indicates that BAI increased in this contrast, "↑" indicates that BAI greatly increased in this contrast, "↓" indicates that BAI decreased in this contrast, "↓↓" indicates that BAI greatly decreased in this contrast,"↔" indicates a miniscule or uncertain change in BAI (i.e., 95% confidence interval includes "0"). "CI" refers to "confidence interval". "Df" refers to "degrees of freedom."

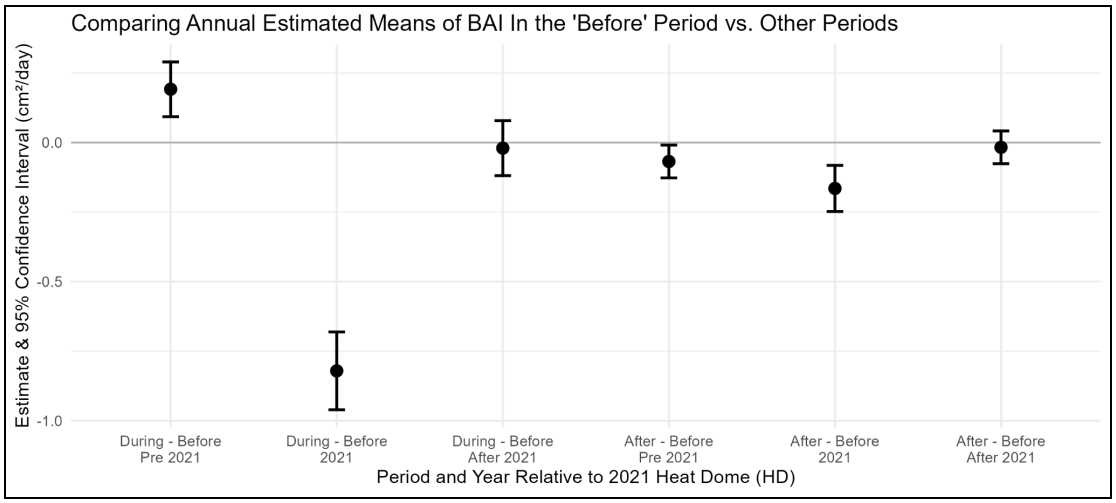

Figure 18: Plot of estimated marginal means for changes in modeled BAI (cm^2/day) between calendar date periods ranging from June 12 - July 12 across 2019-2023 for 6 sample trees. "Pre 2021" refers to the average of 2019 and 2020. "After 2021" refers to the average of 2022 and 2023.

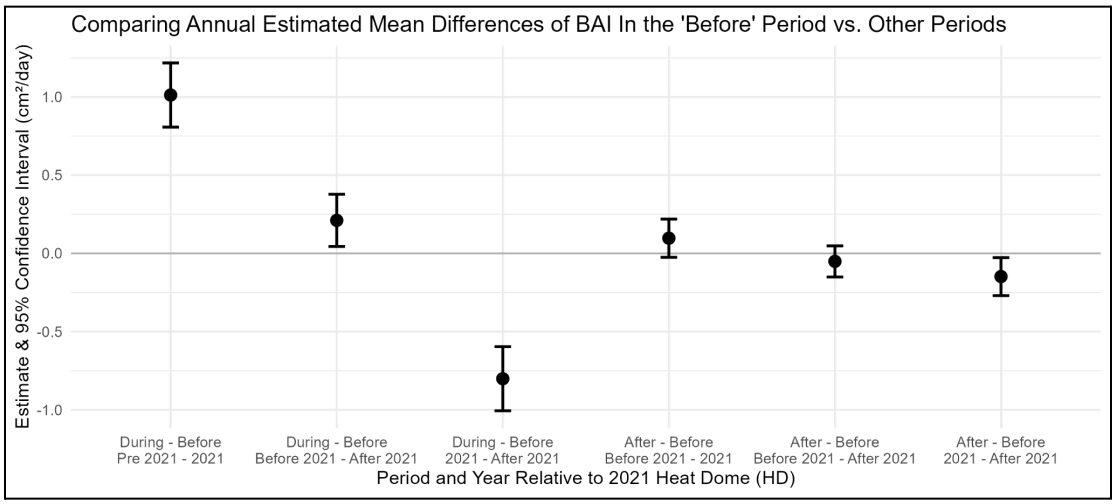

Figure 19: Plot of estimated marginal means for changes in modeled BAI (cm^2/day) differences between calendar date periods and year groups ranging from June 12 - July 12 across 2019-2023 for 6 sample trees. "Pre 2021" refers to the average of 2019 and 2020. "After 2021" refers to the average of 2022 and 2023.

The estimated marginal mean comparisons presented in **Table 10** assume that 2G and OG trees respond the same due to the lack of age class interaction terms in our model. However, 2G exhibited significantly more shrinkage during the Heat Dome than OG trees (**Table 11**). While we cannot say with certainty that OG trees shrank at all during the Heat Dome (95% confidence interval [-0.52, 0.06] cm^2/day), this estimate comes from 2 sample trees that empirically exhibited completely different responses to the Heat Dome (**Figure 15**).

2021 estimated marginal means by period and age class				
Period	**2G estimate**	**2G 95% confidence**	**OG estimate**	**OG 95% confidence**

	(cm^2/day)	interval (cm^2/day)	(cm^2/day)	interval (cm^2/day)
before	0.29	0.12, 0.46	0.59	0.35, 0.84
during	-0.53	-0.75, -0.30	-0.23	-0.52, 0.06
after	0.13	-0.04, 0.30	0.43	0.18, 0.67

Table 11: Estimated marginal means for custom contrasts of modeled BAI (cm2/day) ranging from June 12 - July 12, 2021.

3.3 Trends and observations in tree rings (RQ3)

Table 12 summarizes BAI maxima and minima from tree cores within the last 50 years. The table is truncated to avoid values that might be over-inflated due to rapid growth in the establishment years. Annual BAI (full record for 2G trees, last 75 years for OG trees) is shown in **Figure 20**, and **Figure 21** zooms in on the last 10 years. Cumulative BAI for the full record is shown in **Figure 22**. Only cores for which there are corresponding digital band dendrometers are included in these figures. ID 860 (2G DF) is missing a 2024 growth ring due to its lack of expansion from ice damage.While we could not compare ID 309 (OG DF) to other trees based on dendrometry, the results of our dendrochronological analysis indicate that it performed similar to ID 310 (OG DF) in the long-term record and to ID 655 (2G DF).

As seen in **Figures 13** and **16,** sample trees had high BAI in 2021 until the Heat Dome. **Figure 21** shows the difference in total annual BAI from 2020 to 2021 more clearly, with five sample trees adding more BAI in 2021 than 2020 (IDs 309 [OG DF], 646 & 648 [OG WH], and 654 & 655 [2G DF]). Within this 5-year window, 75% of our sample 2G DF trees added the most total annual increment; ID 656 had its highest BAI in 2020, and IDs 654 and 860 had their highest in 2022–the year right after the Heat Dome. Two trees had their highest annual BAI in 2020 (ID 311 [OG DF] and ID 656 [2G DF]), and two trees had their highest annual BAI in 2022 (IDs 654 and 860 [2G DF]). IDs 654 and 860 were two of only three trees, the third being ID 652 (OG WH), for which BAI exceeded 2021 levels in the subsequent years. All other trees exhibited declines in annual BAI, with some declining year after year.

Minimum and Maximum annual BAI within the Last 50 Years (1974-2024)					
ID	**Maximum BAI (cm^2/year)**	**Minimum BAI (cm^2/year)**	**2021 BAI (cm^2/year)**	**Year of Maximum BAI**	**Year of Minimum BAI**

309	8.05	1.99	6.58	2005	1979
310	9.82	2.03	6.03	1997	1974
311	**33.33**	0.36	25.93	**2020**	1974
646	32.74	4.79	11.50	1997	1987
648	8.75	1.16	4.26	2006	1976
652	10.82	3.44	7.64	1986	1975
654	**47.51**	15.05	41.59	**2022**	2017
655	36.98	5.8	33.91	2013	2008
656	**35.65**	6.76	35.10	**2020**	1978
860	**18.22**	0.95	15.72	**2022**	1975

Table 12: Summary table of minimum and maximum annual BAI(cm2/year) within the last 50 years (1974-2024). Bold values represent metrics that occur within the same time frame as our dendrometry record (2019-2025).

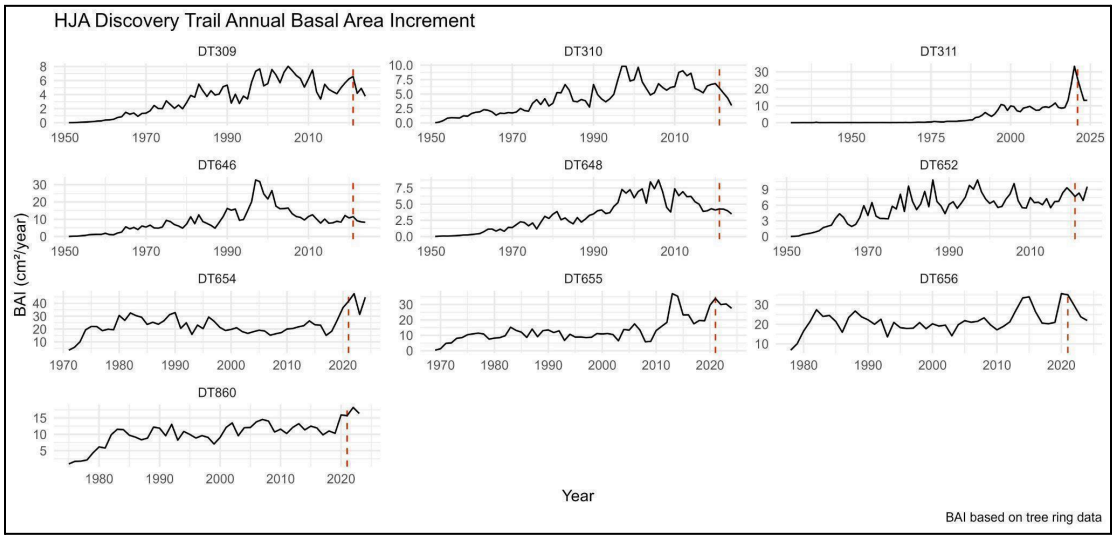

Figure 20: Annual BAI (cm^2/year) for the full record for 2G trees or the most recent 75 years (1950-2025) for OG trees. Red vertical dashed line indicates the year of the Heat Dome (2021).

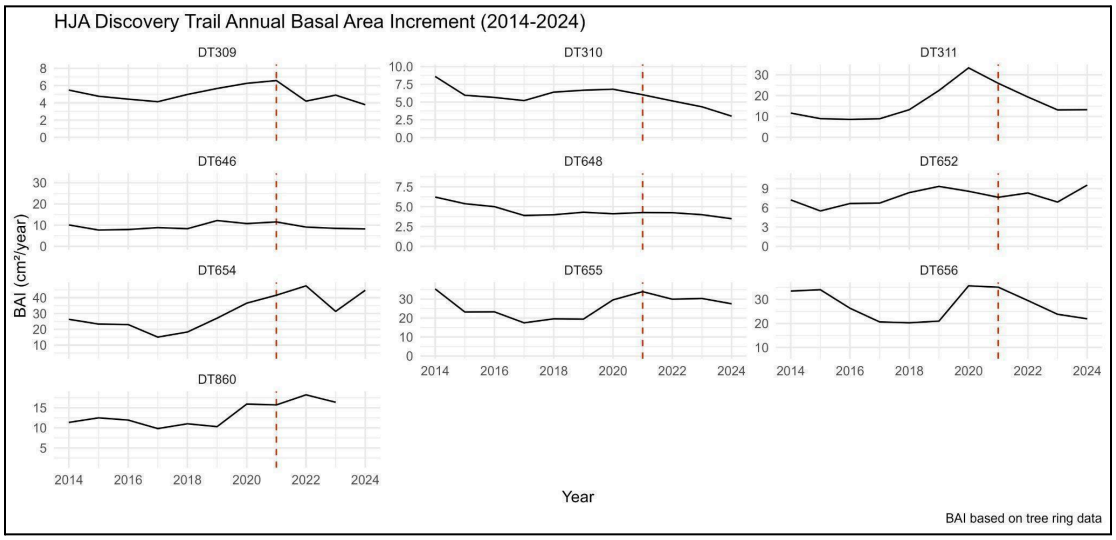

Figure 21: Annual BAI (cm^2/year) for the most recent 10 years (2014-2024). Red vertical dashed line indicates the year of the Heat Dome (2021).

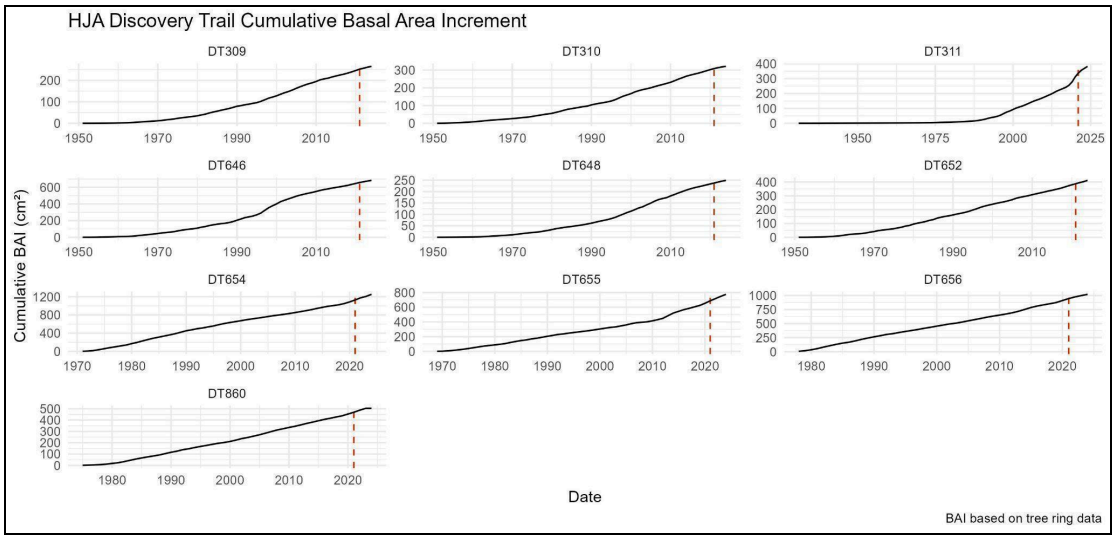

Figure 22: Cumulative annual BAI (cm^2) for the full record for 2G trees or the most recent 75 years (1950-2025) for OG trees. Red vertical dashed line indicates the year of the Heat Dome (2021).

Lastly, to compare latewood distribution within our tree cores, **Figures 23-24** show total ring width, latewood width, and earlywood width on the full timescale as well as the last 10 years. All 2G DF trees except ID 655 exhibit high initial ring widths as they become established, after which their annual ring widths stabilize. ID 655 deviates from this pattern as it adds an uncharacteristically thick ring in 2013 (**Figure 23**).

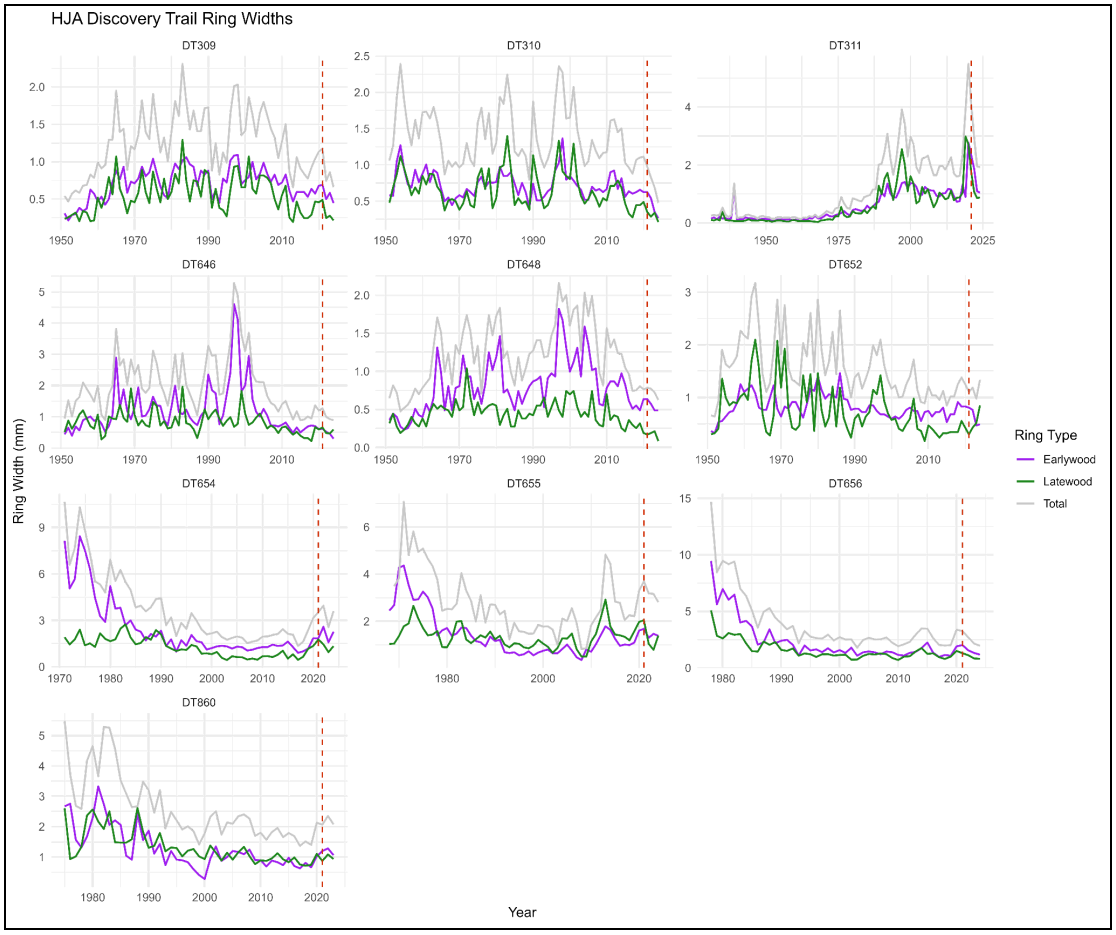

Figure 23: Earlywood, latewood, and total ring width (mm) for the most recent 75 years. Red vertical dashed line indicates the year of the Heat Dome (2021).

In 2021, IDs 646 (OG WH) and 655 (2G DF) put on more latewood than earlywood. This result was characteristic of ID 655 throughout its life history, but ID 646 had only just started to show similar rates of earlywood and latewood additions a few years prior (2019). After 2021, latewood width sharply declines for ID 655 and sharply *inclines* for ID 652 (OG WH).

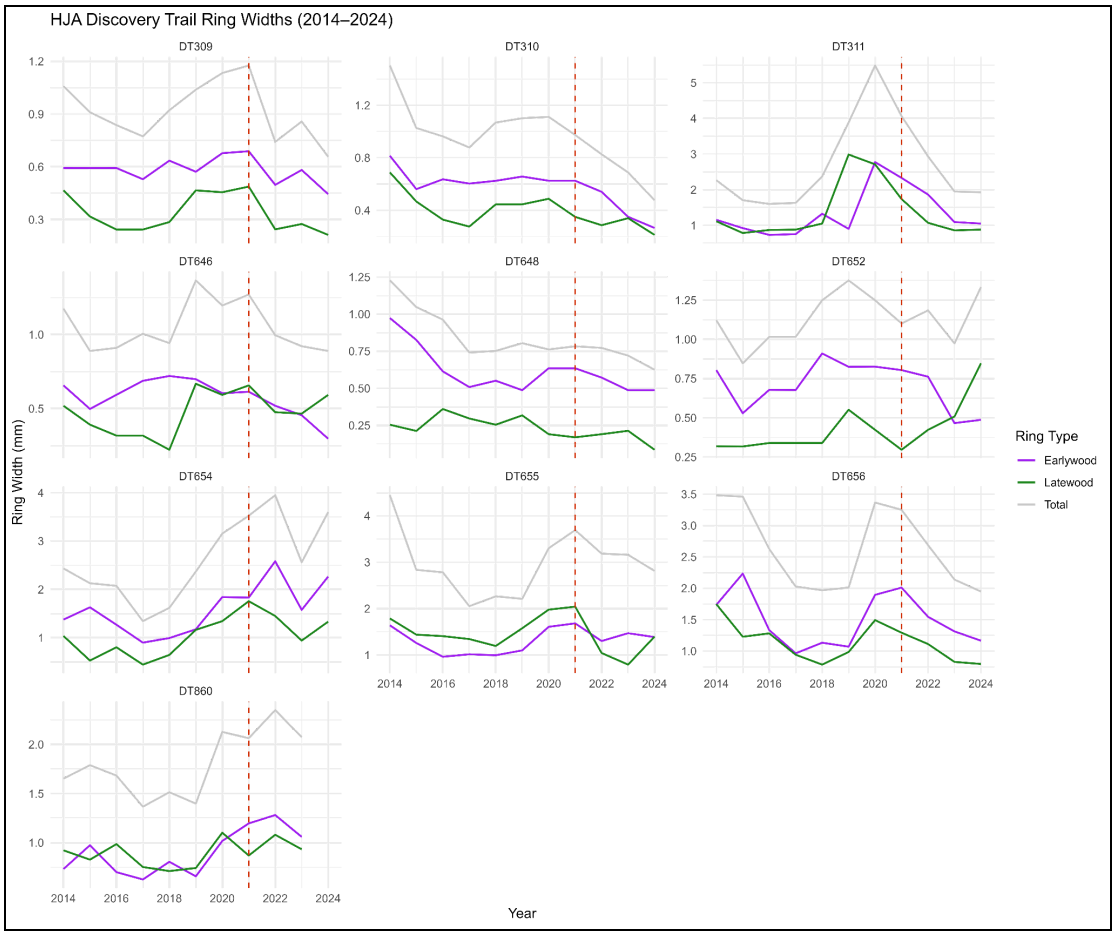

Figure 24: Earlywood, latewood, and total ring width (mm) for the most recent 10 years. Red vertical dashed line indicates the year of the Heat Dome (2021).

4.0 Discussion & Conclusions

4.1 Interpreting Heat Dome impacts on expansion and interactions with microclimate

4.1.1 Interpreting BAI results before and during 2021

The result of analyzing microclimate and dendrometry data as well as modeled BAI affirms that 2021 was indeed unique. Our results support other findings that the Heat Dome led to physiologically severe temperatures and, as such, had severe impacts on trees of the Pacific Northwest (Sibley et al., 2025; Still et al., 2023; White et al. 2023). Within the six trees included in our model (IDs 310, 311 [OG DF], 654, 655, 656, 860 [2G DF]), mean BAI decreases over the calendar period of June 12 to June 28 (“before” versus “during”) significantly more in 2021 than in the years

leading up to and following it (**Table 10, Figure 18**). From this, we can infer that there is less stem expansion happening in 2021 than in the other two year groups. However, because we expected positive increment from early June to late June based on the modeled patterns of growth rate (**Table 7, Figure 13**), the negative increment during the Heat Dome could be more impactful than the data suggest. It is possible that active cell division and drought-induced shrinkage could be happening simultaneously and that the observed results are reflecting *net* shrinkage, not absolute shrinkage (Zweifel et al., 2016).

The decline in BAI associated with the Heat Dome remained significant for at least two weeks after the event concluded (**Table 10**). Prior research has observed that heat stress negatively impacted photosynthesis, transpiration, and stomatal conductance for six weeks after the inciting event (Duarte et al., 2016). In our observations of cumulative BAI, we find lingering impacts of the Heat Dome for the remainder of the 2021 GS (**Figures 16-17, Table 9**). In our analyses of modeled BAI, the significant BAI decline from the "before" period to the "after" period in 2021 was more severe than BAI differences across the same calendar periods in other years. Some decline from the "before" to "after" periods is expected since the date of maximum daily increment will pass between the limits of these two periods (**Table 7**). Therefore, it is the severity of the decline indicating that BAI declines in 2021 was uncharacteristic of typical seasonal decreases in expansion rates and could therefore represent delayed recovery from the Heat Dome (**Table 10, Figures 18-19**).

Much of the existing literature on the Heat Dome emphasizes the drought that preceded the HD to explain the severity of forest responses. While 2021 definitely had the driest GS within our 7-year record, there were still some precipitation events in the days and weeks leading up to the onset of Heat Dome. Overall, there was an intermediate amount of rainfall in the 2021 water year. It was instead air temperature and related metrics like VPD and HDI that deviated the most from historical expectations, leading to an extreme *atmospheric* drought, which is more likely than soil drought to negatively affect gross primary production (Jarecke et al., 2023; Sulman et al., 2016).

The acute effects of temperature are underscored by the steep drop in BAI directly coinciding with the HDI peaks (**Figure 13**). This could mean the daily growth rate slows, there is increased stem contraction due to stem dehydration due to water loss / transpiration, or both (Downes et al., 1999; Zweifel et al., 2016). While HDI remained high for the rest of the summer, we would still expect some latewood expansion through the end of the GS, especially after the albeit minor rain events in July. Instead, for many trees, expansion plateaus (or, in the case of ID 310 [OG DF], declines) until the fall rains begin. This could be an important signal that the stress of the HD either by itself or in conjunction with subsequent heat events prevented stem increment from taking place.

The juxtaposition of the low precipitation in the 2020 water year (**Figure 10**) paired with the high BAI in the 2020 calendar year across all sample IDs (**Figures 16, 21, Table 9**) further reinforces the notion that drought alone should not be used to predict patterns of plant stress (Still et al., 2023b). 2020 was dry but not particularly stressful in terms of temperature, VPD, and HDI (**Figures 7-9; Tables 5-6**). This is not to say precipitation is not highly valuable when interpreting patterns of stem increment. 2019 and 2020 had relatively similar weather patterns, with 2019 being overall less stressful and therefore the least stressful year in our 7-year record in terms of temperature, VPD, and HDI (**Figures 7-9; Tables 5-6**). However, BAI in 2020 was much higher than in 2019 (**Figure 16**). It is possible that this is because 2020 had more rain events in the late spring and mid summer, warranting more research.

Since 2020, GS length seems to decline across all sample trees except in 2024. Warmer springs and summers should lengthen the growing season, but it is important to note that warming climates lead to asynchronous seasonal patterns between periods of general photosynthesis and periods of stem increment wherein periods of stem increment are less affected by warming (Li et al., 2025). This has its limits, as evidenced by the sudden end to the 2021 GS for two of our sample trees.

4.1.2 Interpreting results after 2021

For most sampled trees, observed annual increment since 2021 has declined (**Figures 16, 21, Table 9**). It is challenging to fully attribute this to lingering HD stress; these declines are statistically insignificant for DF and empirically mild for

WH. Moreover, most years since 2021 have been relatively hot and wet (**Figures 7, 10**). The exception to this is 2023, which featured more mild temperatures but more severe droughts. The results of our model confirm the ambiguity of long-term HD impacts. Mean change in modeled BAI in the "before" period versus the "during" period is estimated to be higher in 2019-2020 than in 2022-2023 (**Table 10, Figure 19**). This could indicate inter-annual carry-over impacts as expansion rates may still be returning to pre-Heat Dome levels or that there are other stressful weather events occurring on this small time scale, but our modeled results cannot confirm this with certainty. We estimate that the mean change in BAI from the "before" period to the "after" period is 0.15 cm^2/day lower in 2021 than the mean change in BAI during the same calendar dates of the two years after (**Table 10, Figure 19)**. However, comparisons of mean BAI across the same calendar dates in the other year group combinations (before 2021 - 2021; before 2021 - after 2021) are not significantly different within our model. In other words, our data are reasonably consistent with the null hypothesis that trees recovered quickly and growth was not reduced in the two weeks after the event compared to the same time period in other years. Further investigation of this is warranted given the small sample size of our model as well as the observed declines in BAI in the years following the Heat Dome (**Figure 16**).

The uncommon independence of these heat and drought events have helped us assess their separate effects on tree growth. For example, several individuals experience reduced latewood width, providing additional support for research findings that high summer temperature VPD and heat lead to reductions in latewood widths in a way that cannot be explained by precipitation alone (Jarecke et al., 2024; Ratcliff et al., 2018). On the other hand, BAI was relatively high in 2022 (**Figures 16, 21; Table 9**, **12**) despite having the second most stressful temperature and VPD in our 7-year record (**Figures 7-8**). This year was even the highest BAI year within the last 50 years for two of our cored trees (IDs 654 and 860 [2G DF]) (**Table 12**). 2022 had an exceptionally wet GS relative to all other years, likely contributing to its high BAI. This result invites further research as it is unclear whether these results are due to true increment or stem swelling from the disproportionate amount of rainfall during a historically dry season.

4.1.3 Comparing age class, species, and canopy position

We do not have enough evidence or samples to confidently extrapolate population-level differences between age classes and species, but we are able to describe the patterns observed for these 11 trees at this site. The observed differences in BAI close to the ground versus high into the canopy support the idea that ground-level measurements do not always provide complete insights on plant performance (**Figures 14-16**) (Still et al., 2019). This invites future research to continue exploring how leaf-level gas exchange and shading can contribute to a unique canopy environment.

Regarding species, ID 646 (OG WH) adding the most BAI during the 2021 GS was an unexpected result due to other observed impacts of the Heat Dome (**Figure 16; Table 9**). The result is especially surprising considering that WH was documented to be more sensitive to heat-related foliar mortality (Sibley et al., 2023). While we do not have additional samples or examples to compare this to, we can speculate that since the scorch was mild relative to the other WH trees along the scorch gradient, its impact on overall expansion. Alternatively, this result could be unique to the individual due to genetics or random variation. This uncertainty underscores the value of statistical models and further research. Our single WRC sample (ID 651) only has three years of available BAI data, so we will refrain from making any conclusions about it.

Furthermore, estimated marginal means comparing BAI during the Heat Dome show that shrinkage was significant for 2G DF trees but was more ambiguous for OG DF trees (**Table 11**). These results deviate from our observations of severe contraction for ID 310 (OG DF) (**Figure 15**) as well as the increase in BAI from 2020 to 2021 for IDs 654 and 655 (2G DF) (**Figure 21**). This uncertainty highlights the need for additional samples as our two modeled OG DF trees exhibited opposing empirical responses in high-resolution BAI (**Figure 15**).

The mixed results between 2G and OG trees highlights the potential for future research to more explicitly compare these two age classes. Current research concludes that MOG trees are more resistant and resilient to climate stress (Farinacci et al., 2024; Phillips et al., 2008; Stephenson et al., 2014). These results are typically based

on comparisons to juvenile trees, whereas our youngest trees are still mature. Research comparing mature and old growth tree age classes found that OG trees may have greater capacity to buffer drought impacts due to water stores in the stem (Beedlow et al., 2017). Despite the lack of statistical power in the age comparisons within our model, the results do support this finding.

4.2 Concurrent HJA events potentially contributing to observed results

Influences that were likely to affect the observed results include leaf mortality (scorch), fire, and changes in light availability. High temperatures often lead to foliar damage and mortality, reducing the tree's total capacity to assimilate carbon via photosynthesis (Teskey et al., 2015). A unique outcome of the Heat Dome along the HJA Discovery Trail was a clear gradient of OG WH foliar scorch due to light gaps in the canopies. ID 646 was affected the least, ID 652 was affected the most (but less than other WH in the stand without dendrometers), and ID 648 had intermediate scorch. WH trees were among the most heat-sensitive species at the HJA, as they were more likely to experience scorch under similar conditions of heat and light exposure than other species. On the other hand, across the western region of Oregon and Washington, DF trees were less likely to experience scorch than other trees (Sibley et al., 2025). Observations at the HJA suggest that the health of the most severely-scorched WH individuals continued to decline after other trees started to recover.

While the recent canopy mortality of ID 860 (2G DF) was a result of ice damage rather than scorch, the consequential stagnation in expansion still exemplifies the impacts of leaf death on tree health and growth **(Figures 14, 16**). This was not the only winter event that could affect our observed results. In February 2019, a heavy snow load broke branches and stems and uprooted whole trees, particularly second growth Douglas-firs on the north side of the research plot as well as scattered lower canopy hemlocks in the older stand to the south. This could partially explain why 2019 was a poor growth year for the younger Douglas fir in our second growth stand, as the relatively light but noticeable branch damage on study trees may have initially offset effects of competitive release from surrounding tree mortality. Our

dendrometry results show that 2019 was a poor growth year for most trees except IDs 310 (OG DF) and 646 (OG WH) (**Figure 16, Table 9**).

4.3 Conclusions

Our results represent both the resilience and vulnerabilities of canopy trees at the HJA. The statistically significant reduction in BAI during the Heat Dome affirms our observed results that negative increment in response to the event was immediate. There was individual variation in the severity of this response as well as the rate of recovery afterward. No metric by itself fully predicted BAI, but the patterns discussed here show the profound impacts of extreme heat, VPD, and HDI.

The results of this study highlight just a fraction of the interpretive capabilities of temporally rich data analysis and stress the importance of holistically investigating multiple aspects of microclimate alongside patterns of tree growth. Despite our low sample size, the temporal and vertical gradient of measurements ranging from minutes to years and from the soil to the upper canopy allowed us to infer valuable details and insights on real-time tree responses to adverse climate events. Although interactions between trees and their surrounding climate are specific to the individual, species, and site, there may still be similarities between our results and other DF/WH-dominated mesic forests, of which there are many in the PNW. Thus, we hope that the work presented here provides a methodological framework whereby future researchers can similarly synthesize multiple modes of data to explore the relationships between tree expansion and weather across several time scales for other species, ecosystems, and times. Such investigations may better prepare forest managers, policymakers, and other community stakeholders to adjust to a rapidly changing world.

5.0 Data Availability

Data for this study came from the HJA Provisional Data Portal (Andrews Forest Program, n.d.), the National Atmospheric Deposition Program (National Atmospheric

Deposition Program, 2022), and HJA databases that had undergone quality control checks beyond what is available for provisional data (e.g., Daly et al., 2025).

6.0 Code Availability

Code used for this analysis will become available on a GitHub reposity at github.com/gabhrieljohn/GJ_OSU_Thesis.

7.0 References

Acosta-Hernández, A.C., Padilla-Martínez, J.R., Hernández-Díaz, J.C., Prieto-Ruiz, J.A., Goche-Telles, J.R., Nájera-Luna, J.A. & Pompa-García, M. (2020) Influence of climate on carbon sequestration in conifers growing under contrasting hydro-climatic conditions. *Forests*, 11, 1134. https://doi.org/10.3390/f11111134

Allen, C.D., Macalady, A.K., Chenchouni, H., Bachelet, D., McDowell, N.G., Vennetier, M., Kitzberger, T., Rigling, A., Breshears, D.D., Hogg, E.H., González, P., Fensham, R.J., Zhang, Z., Castro, J., Demidova, N., Lim, J.H., Allard, G., Running, S.W., Semerci, A. & Cobb, N.S. (2010) A global overview of drought and heat-induced tree mortality reveals emerging climate change risks for forests. *Forest Ecology and Management*, 259, 660–684. https://doi.org/10.1016/j.foreco.2009.09.001

Andrews Forest Program (n.d.) Provisional Data Portal. Andrews Forest Research Program. https://andrewsforest.oregonstate.edu/data/streaming/provisional-data-portal

Andrews Forest Program via CC-BY (n.d.) Provisional Real-Time Data Graphs and Other Data Products. Andrews Forest Research Program https://andrewsforest.oregonstate.edu/data/streaming

Aryal, S., Häusser, M., Grießinger, J., Fan, Z. & Bräuning, A. (2024) dendRoAnalyst: A Tool for Processing and Analyzing Dendrometer Data. R package version 0.1.5. https://CRAN.R-project.org/package=dendRoAnalyst

Balducci, L., Deslauriers, A., Rossi, S. & Giovannelli, A. (2019) Stem cycle analyses help decipher the nonlinear response of trees to concurrent warming and drought. *Annals of Forest Science*, 76, 3. https://doi.org/10.1007/s13595-019-0870-7

Batavia, C. & Nelson, M.P. (2018) Translating climate change policy into forest management practice in a multiple-use context: the role of ethics. Climatic Change, 148, 81–94. https://doi.org/10.1007/s10584-018-2186-2

Brackett, A.E., Still, C.J. & Puettmann, K.J. (2024) Residual canopy cover provides buffering of near-surface temperatures, but benefits are limited under extreme conditions. Canadian Journal of Forest Research, 54, 1018–1031. https://doi.org/10.1139/cjfr-2023-0268

Breshears, D.D., Adams, H.D., Eamus, D., McDowell, N., Law, D.J., Will, R.E., Williams, A.P. & Zou, C.B. (2013) The critical amplifying role of increasing

atmospheric moisture demand on tree mortality and associated regional die-off. Frontiers in Plant Science, 4, 266. https://doi.org/10.3389/fpls.2013.00266

Breshears, D.D., Fontaine, J.B., Ruthrof, K.X., Field, J.P., Feng, X., Burger, J.R., Law, D.J., Kala, J. & Hardy, J.E.S. (2021) Underappreciated plant vulnerabilities to heat waves. New Phytologist, 231, 32–39. https://doi.org/10.1111/nph.17348

Bunn, A.G. (2010) Statistical and visual crossdating in R using the dplR library. Dendrochronologia, 28(4), 251-258. https://doi.org/10.1016/j.dendro.2009.12.001

Bunn, A.G., Korpela, M., Biondi, F., Campelo, F., Klesse, S., Mérian, P., Qeadan, F., Zang, C. (2025) dplR: Dendrochronology Program Library in R. R package version 1.7.8, https://CRAN.R-project.org/package=dplR

Campbell, R., McCarroll, D., Robertson, I., Loader, N.J., Grudd, H. & Gunnarson, B. (2011) Blue intensity in Pinus sylvestris tree rings: a manual for a new palaeoclimate proxy. Tree-Ring Research, 67, 127–134. https://doi.org/10.3959/2010-13.1

Chang, M., Erikson, L., Araújo, K., Asinas, E.N., Chisholm Hatfield, S., Crozier, L.G., Fleishman, E., Greene, C.S., Grossman, E.E., Luce, C., Paudel, J., Rajagopalan, K., Rasmussen, E., Raymond, C., Reyes, J.J. & Shandas, V. (2023) Ch. 27. Northwest. In: *Fifth National Climate Assessment* (eds Crimmins, A.R., Avery, C.W., Easterling, D.R., Kunkel, K.E., Stewart, B.C. & Maycock, T.K.), U.S. Global Change Research Program, Washington, DC. https://doi.org/10.7930/NCA5.2023.CH27

Dai, L., Jia, J., Yu, D., Lewis, B., Zhou, L., Zhou, W., Zhao, W. & Jiang, L. (2013) Effects of climate change on biomass carbon sequestration in old-growth forest ecosystems on Changbai Mountain in Northeast China. *Forest Ecology and Management*, 300, 106–116. https://doi.org/10.1016/j.foreco.2012.06.046

Daly, C., Schulze, M., McKee, W. (2025) Air temperature, relative humidity, dewpoint temperature, water vapor pressure deficit, and atmospheric pressure data from benchmark stations at the HJ Andrews Experimental Forest, 1957 to present. Long-Term Ecological Research. Forest Science Data Bank, Corvallis, OR. [Database]. https://doi.org/10.6073/pasta/5d4ab4b210165d6e860ebe58e0579e4e.

Davis, S.J., Dodder, R.S., Turner, D.D., Azevedo, I.M.L., Bazilian, M., Bistline, J., Carley, S., Clack, C.T.M., Fargione, J.E., Grubert, E., Hill, J., Hollis, A.L., Jenn, A., Jones, R.A., Masanet, E., Mayfield, E.N., Muratori, M., Peng, W. & Sellers, B.C. (2023) Ch. 32. Mitigation. In: *Fifth National Climate Assessment* (eds Crimmins, A.R., Avery, C.W., Easterling, D.R., Kunkel, K.E., Stewart, B.C. & Maycock, T.K.), U.S. Global Change Research Program, Washington, DC. https://doi.org/10.7930/NCA5.2023.CH32

Deslauriers, A., Rossi, S., Turcotte, A., Morin, H. & Krause, C. (2011) A three-step procedure in SAS to analyze the time series from automatic dendrometers. *Dendrochronologia*, 29, 151–161. https://doi.org/10.1016/j.dendro.2011.01.008

Doolittle, C. J. (2025). The Local Neighborhood Interactions Shaping Tree

Communities Through Ecological Disturbance and Environmental Change. PhD dissertation. Marquette University, Milwaukee, WI.

Downes, G.M., Beadle, C.L. & Worledge, D. (1999) Daily stem growth patterns in irrigated *Eucalyptus globulus* and *E. nitens* in relation to climate. *Trees*, 14, 102–111. https://doi.org/10.1007/pl00009752

Duarte, A.G., Katata, G., Hoshika, Y., Hossain, M., Kreuzwieser, J., Arneth, A. & Ruehr, N.K. (2016) Immediate and potential long-term effects of consecutive heat waves on the photosynthetic performance and water balance in Douglas-fir. *Journal of Plant Physiology*, 205, 57–66. https://doi.org/10.1016/j.jplph.2016.08.012

Entwurf (2019) https://ecomatik.de/site/assets/files/13369/usermanual_dc3.pdf

ESIP EnviroSensing Cluster (2014) Community Wiki Document, "Best practices for sensor networks and sensor data management", Federation of Earth Science Information Partners. http://wiki.esipfed.org/index.php/EnviroSensing_Cluster

ETI Instrument Systems. (2020). NOAH IV™ Total Precipitation Gauge: Operation and Maintenance Manual. NADP Program Office, Wisconsin State Laboratory of Hygiene. https://nadp.slh.wisc.edu/wp-content/uploads/2021/09/ETI_NOAHIV_Manual.pdf

Fleishman, E., Rupp, D.E., Loikith, P.C., Bumbaco, K.A., & O'Neill, L.W. (2025). Synthesis of Publications on the Anomalous June 2021 Heat Wave in the Pacific Northwest of the United States and Canada. Bulletin of the American Meteorological Society, 106(6), E1155-E1174. https://doi.org/10.1175/BAMS-D-24-0188.1

Garnier, S., Ross, N., Rudis, R., Camargo, A. P., Sciaini, M., & Scherer, C. (2024). viridis: Colorblind-friendly color maps for R (Version 0.6.5). Retrieved from https://CRAN.R-project.org/package=viridis

Grossiord, C., Buckley, T.N., Cernusak, L.A., Novick, K.A., Poulter, B., Siegwolf, R.T.W., Sperry, J.S. & McDowell, N.G. (2020) Plant responses to rising vapor pressure deficit. *New Phytologist*, 226, 1550–1566. https://doi.org/10.1111/nph.16485

Haeni, M., Knüsel, S., Peters, R.L. & Zweifel, R. (2020) treenetproc – clean, process and visualise dendrometer data. R package v.0.1.4. Github repository. https://github.com/treenet/treenetproc

Hammond, W.M., Williams, A.P., Abatzoglou, J.T. et al. (2022) Global field observations of tree die-off reveal hotter-drought fingerprint for Earth's forests. *Nature Communications*, 13, 1761. https://doi.org/10.1038/s41467-022-29289-2

Harrington, C.A., Gould, P.J., Cronn, R. (2023) Site and provenance interact to influence seasonal diameter growth of Pseudotsuga menziesii. Frontiers in Forests and Global Change. 6:1173707. https://doi.org/10.3389/ffgc.2023.1173707

Heeter, K.J., Harley, G.L., Abatzoglou, J.T., Anchukaitis, K.J., Cook, E.R., Coulthard, B.L., Dye, L.A. & Homfeld, I.K. (2023) Unprecedented 21st century heat across the Pacific Northwest of North America. *npj Climate and Atmospheric Science*, 6, 1–9. https://doi.org/10.1038/s41612-023-00340-3

Holmes, R.L., Adams, R.K., & Fritts, H.C. (1986) Tree-Ring Chronologies of Western North America: California, Eastern Oregon and Northern Great Basin with Procedures Used in the Chronology Development Work Including User's Manuals for Computer Programs COFECHA and ARSTAN. Laboratory of Tree-Ring Research, University of Arizona, Tucson. Available at https://repository.arizona.edu/handle/10150/304672

Italiano, S.S.P., Camarero, J.J., Colangelo, M., Borghetti, M., Castellaneta, M., Pizarro, M. & Ripullone, F. (2023) Assessing forest vulnerability to climate change combining remote sensing and tree-ring data: issues, needs and avenues. *Forests*, 14, 1138. https://doi.org/10.3390/f14061138

Jarecke, K.M., Hawkins, L.R., Bladon, K.D. & Wondzell, S.M. (2023) Carbon uptake by Douglas-fir is more sensitive to increased temperature and vapor pressure deficit than reduced rainfall in the western Cascade Mountains, Oregon, USA. *Agricultural and Forest Meteorology*, 329, 109267. https://doi.org/10.1016/j.agrformet.2022.109267

Johnson, K.N. & Swanson, F.J. (2009) Historical context of old-growth forests in the Pacific Northwest--policy, practices, and competing worldviews. In: *Old Growth in a New World: A Pacific Northwest Icon Reexamined* (eds Spies, T.A. & Duncan, S.L.), pp. 12–28. Island Press, Washington, DC; Covelo, CA.

Klein, T., Torres-Ruiz, J.M. & Albers, J.J. (2022) Conifer desiccation in the 2021 NW heatwave confirms the role of hydraulic damage. Tree Physiology, 42, 722–726. https://doi.org/10.1093/treephys/tpac007

Knüsel, S., Peters, R.L., Haeni, M., Wilhelm, M. & Zweifel, R. (2021) Processing and extraction of seasonal tree physiological parameters from stem radius time series. *Forests*, 12, 765. https://doi.org/10.3390/f12060765

Kunert, N., Hajek, P., Hietz, P., Morris, H., Rosner, S. & Tholen, D. (2022) Summer temperatures reach the thermal tolerance threshold of photosynthetic decline in temperate conifers. *Plant Biology*, 24, 1254–1261. https://doi.org/10.1111/plb.13349

Laird, N.M. & Ware, J.H. (1982) Random-effects models for longitudinal data. Biometrics, 38, 963–974.

Larsson, L. (2005) CDendro & CooRecorder program package, version 9.8.1. https://www.cybis.se/forfun/dendro

Lenth, R. (2025) emmeans: Estimated Marginal Means, aka Least-Squares Means. R package version 1.11.0. https://CRAN.R-project.org/package=emmeans

Li, W., Yue, F., Wang, C., Liao, J. & Zhang, X. (2022) Climatic influences on intra-annual stem variation of Larix principis-rupprechtii in a semi-arid region. Frontiers in Forests and Global Change, 5, 948022. https://doi.org/10.3389/ffgc.2022.948022

Li, X., Piao, S., Huntingford, C., Peñuelas, J., Yang, H., Xu, H., Chen, A., Friedlingstein, P., Keenan, T.F., Sitch, S., Wang, X., Zscheischler, J., Mahecha, M.D. (2023) Global variations in critical drought thresholds that impact vegetation. National Science Review, 10(5):nwad049. https://doi.org/10.1093/nsr/nwad049

Marks, S., Surfleet, C., & Malama, B. (2024). Estimating and modeling Pinus contorta transpiration in a montane meadow using sap-flow measurements.

Forests, 15, 1786. https://doi.org/10.3390/f15101786
Martin, J., Looker, N., Hoylman, Z., Jencso, K. & Hu, J. (2017) Hydrometeorology organizes intra-annual patterns of tree growth across time, space and species in a montane watershed. New Phytologist, 215, 1387–1398. https://doi.org/10.1111/nph.14668
Meko, D.M. & Baisan, C.H. (2001) Pilot study of latewood-width of conifers as an indicator of variability of summer rainfall in the North American monsoon region. International Journal of Climatology, 21, 697–708. https://doi.org/10.1002/joc.646
Müller, K. (2020). here: A simpler way to find your files (Version 1.0.1). Retrieved from https://CRAN.R-project.org/package=here
National Atmospheric Deposition Program (NRSP-3) (2022) NADP Program Office, Wisconsin State Laboratory of Hygiene, 465 Henry Mall, Madison, WI 53706. https://nadp.slh.wisc.edu/
Novick, K.A., Ficklin, D.L., Grossiord, C., Konings, A.G., Martínez-Vilalta, J., Sadok, W., Trugman, A.T., Williams, A.P., Wright, A.J., Abatzoglou, J.T., Dannenberg, M.P., Gentine, P., Guan, K., Johnston, M.R., Lowman, L.E.L., Moore, D.J.P. & McDowell, N.G. (2024) The impacts of rising vapour pressure deficit in natural and managed ecosystems. *Plant, Cell & Environment*, 47, 3561–3589. https://doi.org/10.1111/pce.14846
R Core Team (2024) *R: A Language and Environment for Statistical Computing*. R Foundation for Statistical Computing, Vienna, Austria. https://www.R-project.org/
Rastogi, B., Berkelhammer, M., Wharton, S., Whelan, M.E., Meinzer, F.C., Noone, D. & Still, C.J. (2018) Ecosystem fluxes of carbonyl sulfide in an old-growth forest: temporal dynamics and responses to diffuse radiation and heat waves. *Biogeosciences*, 15, 7127–7139. https://doi.org/10.5194/bg-15-7127-2018
Regent Instruments Inc. (n.d.). WinDENDRO [Computer software].
Reich, P.B., Luo, Y., Bradford, J.B., Poorter, H., Perry, C.H. & Oleksyn, J. (2014) Temperature drives global patterns in forest biomass distribution in leaves, stems, and roots. *Proceedings of the National Academy of Sciences USA*, 111, 13721–13726. https://doi.org/10.1073/pnas.1216053111
Restaino, C. M., Peterson, D. L., & Littell, J. (2016). Increased water deficit decreases Douglas-fir growth throughout western US forests. Proceedings of the National Academy of Sciences of the United States of America, 113, 9557–9562. https://doi.org/10.1073/pnas.1602384113
Phillips, N.G., Buckley, T.N. & Tissue, D.T. (2008) Capacity of old trees to respond to environmental change. Journal of Integrative Plant Biology, 50, 1355–1364. https://doi.org/10.1111/j.1744-7909.2008.00746.x
Pinheiro, J., Bates, D. & R Core Team (2024) *nlme: Linear and Nonlinear Mixed Effects Models*. R package version 3.1-166. https://CRAN.R-project.org/package=nlme
Pinheiro, J.C. & Bates, D.M. (2000) *Mixed-Effects Models in S and S-PLUS*. Springer, New York. https://doi.org/10.1007/b98882
Rupsys, P., Bartkevicius, E. & Petrauskas, E. (2011) A univariate stochastic Gompertz model for tree diameter modeling. *Trends in Applied Sciences*

Research, 6, 134–153. https://scialert.net/abstract/?doi=tasr.2011.134.153

Salomón, R.L., Peters, R.L., Zweifel, R., Sass‐Klaassen, U., Stegehuis, A.I., Smiljanić, M., Poyatos, R., Babst, F., Cienciala, E., Fonti, P., Lerink, B., Lindner, M., Vilalta, J., Mencuccini, M., Nabuurs, G., Van Der Maaten, E., Von Arx, G., Bär, A., Akhmetzyanov, L., ... Steppe, K. (2022) The 2018 European heatwave led to stem dehydration but not to consistent growth reductions in forests. *Nature Communications*, 13, 1. https://doi.org/10.1038/s41467-021-27579-9

Sheldon, W., Chamblee, J. & Cary, R.H. (2013) GCE Data Toolbox for MATLAB - a software framework for automating environmental data processing, quality control and documentation. AGU Fall Meeting Abstracts, 2013, ED53B-0641. https://ui.adsabs.harvard.edu/abs/2013AGUFMED53B0641S

Sibley, A., Still, C., Gregory, M., Harrington, C., Shaw, D., Ferrari, N., Dye, A., Schulze, M., Howe, G., Rupp, D.E., Daly, C., DePinte, D., Naficy, C.E., Hart, C. & Bell, D.M. (2025) Extreme heatwave causes immediate, widespread mortality of forest canopy foliage, highlighting modes of forest sensitivity to extreme heat. *Global Change Biology*, 31, e70571. https://doi.org/10.1111/gcb.70571

Slowikowski, K. (2024). ggrepel: Automatically position non-overlapping text labels with 'ggplot2' (Version 0.9.6). Retrieved from https://CRAN.R-project.org/package=ggrepel

Stephenson, N.L., Das, A.J., Condit, R., Russo, S.E., Baker, P.J., Beckman, N.G., Coomes, D.A., Lines, E.R., Morris, W.K., Rüger, N., Álvarez, E., Blundo, C., Bunyavejchewin, S., Chuyong, G., Davies, S.J., Duque, Á., Ewango, C.N., Flores, O., Franklin, J.F., ... Zavala, M.A. (2014) Rate of tree carbon accumulation increases continuously with tree size. *Nature*, 507, 90–93. https://doi.org/10.1038/nature12914

Still, C.J., Kim, Y., Heffernan, E., Schulze, M.D., Sibley, A. & Kennedy, A.M. (2023a) Meteorological data from the Discovery Tree at the Andrews Experimental Forest, 2015 to present ver 3. Environmental Data Initiative. https://doi.org/10.6073/pasta/88040f52946c09c74ac0bfc2a3167717

Still, C., Powell, R., Aubrecht, D., Kim, Y., Helliker, B., Roberts, D., Richardson, A.D. & Goulden, M. (2019) Thermal imaging in plant and ecosystem ecology: applications and challenges. Ecosphere, 10, e02768. https://doi.org/10.1002/ecs2.2768

Still, C.J., Sibley, A., Depinte, D., Busby, P.E., Harrington, C.A., Schulze, M., Shaw, D.R., Woodruff, D.R., Rupp, D.E., Daly, C., Hammond, W.P. & Page, G. (2023b) Causes of widespread foliar damage from the June 2021 Pacific Northwest Heat Dome: more heat than drought. *Tree Physiology*, 43, 203–209. https://doi.org/10.1093/treephys/tpac143

Swanson, F.J. (2023) The H.J. Andrews Experimental Forest Long-Term Ecological Research Program, Oregon, USA: a historical biocultural perspective. In: *Field Environmental Philosophy. Ecology and Ethics*, Vol. 5:32 (eds Rozzi, R., Tauro, A., Avriel-Avni, N., Wright, T. & May, R.H. Jr.), pp. 532–554. https://doi.org/10.1007/978-3-031-23368-5_32

Teskey, R., Wertin, T., Bauweraerts, I., Ameye, M., Mcguire, M.A. & Steppe, K.

(2015) Responses of tree species to heat waves and extreme heat events. *Plant, Cell & Environment*, 38, 1699–1712. https://doi.org/10.1111/pce.12417

Thompson, V., Kennedy-Asser, A.T., Vosper, E., Lo, Y.T.E., Huntingford, C., Andrews, O., Collins, M., Hegerl, G.C. & Mitchell, D. (2022) The 2021 western North America heat wave among the most extreme events ever recorded globally. *Science Advances*, 8, eabm6860. https://doi.org/10.1126/sciadv.abm6860

Uchytil, R. J. (1991) Pseudotsuga menziesii var. menziesii, coast Douglas-fir. In: Fire Effects Information System [Online]. U.S. Department of Agriculture, Forest Service, Rocky Mountain Research Station, Fire Sciences Laboratory. Available at https://research.fs.usda.gov/feis/species-reviews/psemenm

Wang, Y., Xing, C., Gu, Y., Zhou, Y., Song, J., Zhou, Z., Song, J. & Gao, J. (2023) Responses and post-recovery of physiological traits after drought–heatwave combined event in 12 urban woody species. *Forests*, 14, 1429. https://doi.org/10.3390/f14071429

White, R.H., Anderson, S., Booth, J.F., Braich, G., Draeger, C., Fei, C., Harley, C.D.G., Henderson, S.B., Jakob, M., Lau, C., Admasu, L.M., Narinesingh, V., Rodell, C., Roocroft, E., Weinberger, K.R. & West, G. (2023) The unprecedented Pacific Northwest heatwave of June 2021. Nature Communications, 14, 727. https://doi.org/10.1038/s41467-023-36289-3

Wickham, H., Averick, M., Bryan, J., Chang, W., McGowan, L. D., François, R., Grolemund, G., Hayes, A., Henry, L., Hester, J., Kuhn, M., Pedersen, T. L., Miller, E., Bache, S. M., Müller, K., Ooms, J., Robinson, D., Seidel, D. P., Spinu, V., Takahashi, K., Vaughan, D., Wilke, C., Woo, K., & Yutani, H. (2019). Welcome to the tidyverse. Journal of Open Source Software, 4, 1686. https://doi.org/10.21105/joss.01686

Williams, A.P., Allen, C.D., Macalady, A.K., Griffin, D., Woodhouse, C.A., Meko, D.M., Swetnam, T.W., Rauscher, S.A., Seager, R., Grissino-Mayer, H.D., Dean, J.S., Cook, E.R., Gangodagamage, C., Cai, M. & McDowell, N.G. (2013) Temperature as a potent driver of regional forest drought stress and tree mortality. *Nature Climate Change*, 3, 292–297. https://doi.org/10.1038/nclimate1693

Yi, C., Hendrey, G., Niu, S., McDowell, N. & Allen, C.D. (2022) Tree mortality in a warming world: causes, patterns, and implications. *Environmental Research Letters*, 17, 030201. https://doi.org/10.1088/1748-9326/ac507b

Zweifel, R., Haeni, M., Buchmann, N. & Eugster, W. (2016) Are trees able to grow in periods of stem shrinkage? *New Phytologist*, 211, 839–849. https://doi.org/10.1111/nph.13995

8.0 Summary Of Abbreviated Terminology

DF = Douglas-fir

DSCMET = Discovery Tree Meteorological Station

GS = growing season

HJA = HJ Andrews Experimental Forest

MOG = mature and old-growth

OG = old-growth

PNW = Pacific Northwest

PRIMET = Primary Meteorological Station

SDH = stress degree hours

SVH = stress VPD hours

SWC = soil water content

VPD = vapor pressure deficit

WH = western hemlock